The Astrophysical Journal, 904:150 (20pp), 2020 December 1 https://doi.org/10.3847/1538-4357/abc1e6

Supermassive Black Hole Fueling in IllustrisTNG: Impact of Environment

Aklant K. Bhowmick, Laura Blecha, and July Thomas
Department of Physics, University of Florida, Gainesville, FL 32611, USA
Received 2020 June 27; revised 2020 October 6; accepted 2020 October 14; published 2020 November 30

Abstract

We study the association between active galactic nuclei (AGNs) and environment at scales of 0.01–1 h^{-1} Mpc in the IllustrisTNG simulated universe (TNG100). We identify supermassive black hole (BH) pairs and multiples within scales of 0.01, 0.1, and 1 h^{-1} Mpc and examine their AGN activity in relation to randomly selected pairs and multiples. The number density of BHs in TNG100 is $n = 0.06\,h^3$ Mpc^{-3} at $z \lesssim 1.5$ ($n = 0.02\,h^3$ Mpc^{-3} at $z = 3$). About ∼10% and ∼1% of these BHs live in pairs and multiples, respectively, within 0.1 h^{-1} Mpc scales. These systems have enhanced likelihood (up to factors of 3–6) of containing high Eddington ratio ($\eta \gtrsim 0.7$) AGNs compared to random pairs and multiples. Conversely, the likelihood of an AGN to live in 0.1 h^{-1} Mpc scale BH systems is also higher (by factors ∼4 for $\eta \gtrsim 0.7$) compared to random pairs and multiples. ∼10% of ultra-hard X-ray selected AGNs in TNG100 have detectable 2–10 keV AGN companions on 0.1 h^{-1} Mpc scales, consistent with observations. On larger spatial scales (∼1 h^{-1} Mpc), however, no significant enhancements in AGN activity exist, even at high Eddington ratios. This implies that small-scale ($\lesssim$0.1 h^{-1} Mpc) AGN enhancement is likely driven by galaxy interactions and mergers. Nonetheless, the overall percentage of AGNs living in $\lesssim$0.1 h^{-1} Mpc scale multiples is still subdominant ($\lesssim$40%). Furthermore, the associated Eddington ratio enhancements of BH systems (as well as merging BHs) is only up to factors of ∼2–3. Our results support the existence of merger-AGN connection in TNG100. However, it plays a relatively minor role in fueling the AGN population.

Unified Astronomy Thesaurus concepts: Supermassive black holes (1663); Active galactic nuclei (16)

1. Introduction

It is well established that supermassive black holes (BHs) reside at the centers of almost all nearby massive galaxies (Kormendy & Richstone 1992; Harms et al. 1994; Miyoshi et al. 1995). We also know that a small fraction of galaxies have bright nuclei referred to as active galactic nuclei, or AGNs, which are powered by accreting supermassive BHs. Determining the dominant mechanisms that drive AGN fueling and their connection to BH-galaxy co-evolution is an ongoing challenge.

Fueling BH accretion requires the availability of cold gas with low angular momentum. The large-scale ($\gtrsim$1 h^{-1} Mpc) and small-scale ($\lesssim$0.1 h^{-1} Mpc) environments of AGNs can therefore provide important clues about their fueling mechanisms. For example, the weak dependence seen for the observed large-scale clustering on AGN luminosity (Li et al. 2006; Krumpe et al. 2018; Wang & Li 2019; Powell et al. 2020) implies that more massive haloes do not necessarily host more luminous AGNs, which is also seen in the large scatter in the AGN luminosity versus host halo mass relations in hydrodynamic simulations (Bhowmick et al. 2019). Numerous mechanisms may contribute to AGN triggering. On the one hand, this can be driven by secular processes occurring within the host galaxy such as supernova winds (Chen et al. 2009; Kumar & Johnson 2010) and hydrodynamic instabilities (Kormendy & Kennicutt 2004; Bournaud et al. 2011). On the other hand, external disturbances to the host galaxy, such as tidal torques generated during galaxy interactions and mergers are also very promising candidates, particularly in gas-rich, major mergers (e.g., Barnes & Hernquist 1996; Di Matteo et al. 2005; Hopkins et al. 2008; Blecha et al. 2013; Capelo et al. 2015; Yang et al. 2019).

Currently, there is no clear consensus about whether galaxy mergers or secular processes are the dominant drivers of BH fueling. A vast majority of AGN host galaxies do not exhibit any evidence of recent mergers (Villforth et al. 2014; Marian et al. 2019). Several works analyzing the morphologies of the host galaxies found no significant differences in the "merger fractions" between active and inactive galaxies (e.g., Gabor et al. 2009; Cisternas et al. 2011; Kocevski et al. 2012; Schawinski et al. 2012; Villforth et al. 2014, 2017; Marian et al. 2019; Zakamska et al. 2019; Zhao et al. 2019). In contrast, many other works have also found that galaxies that do exhibit signatures of mergers or interactions have higher AGN fractions compared to those that do not (e.g., Liu et al. 2011; Silverman et al. 2011; Ellison et al. 2011, 2013; Lackner et al. 2014; Satyapal et al. 2014; Weston et al. 2017; Goulding et al. 2018; Ellison et al. 2019). Potential signatures of the AGN-merger connection can also be seen in small-scale quasar clustering measurements of binary quasar pairs, wherein enhanced clustering amplitude is reported at small scales (few tens of kiloparsecs), as compared to extrapolations from large-scale clustering (Schneider et al. 2000; Hennawi et al. 2006; Kayo & Oguri 2012; McGreer et al. 2016; Eftekharzadeh et al. 2017). However, observational studies of merger-triggered AGNs are associated with several challenges. For one, the AGN luminosity can make it difficult to identify morphological merger signatures in the host galaxy. Galaxy mergers may also create a significant amount of quasar obscuration, as seen in both simulations (e.g., Hopkins et al. 2006; Snyder et al. 2013; Blecha et al. 2018) and observations (e.g., Sanders et al. 1988; Sanders & Mirabel 1996; Veilleux et al. 2009; Ricci et al. 2017); this can make it difficult to identify merger-triggered AGNs. The resulting systematic biases could potentially explain the seemingly conflicting results in the existing literature; this is corroborated by the growing evidence of high merger fractions among obscured AGNs (e.g., Urrutia et al. 2008; Glikman et al. 2015; Kocevski et al. 2015; Koss et al. 2018; Gao et al. 2020).

Cosmological hydrodynamic simulations have also shown statistically robust evidence of the presence of the merger-AGN connection. A recent study by McAlpine et al. (2020) looked at merger fractions of AGN hosts as well as AGN fractions of merging galaxies within the EAGLE (Evolution and Assembly of GaLaxies and their Environments) simulation (Schaye et al. 2015) and demonstrated the existence of a merger-AGN connection, though they also found that merger-driven activity does not contribute significantly to the overall growth history of the BH populations. Using data from the MassiveBlackII simulation, (Bhowmick et al. 2019, 2020) demonstrated that merger-driven AGN activity also leads to the formation of systems of multiple active AGNs. Additionally, in a companion paper to the present work, J. Thomas et al. (2020, in preparation) are using very high time resolution data from IllustrisTNG to quantify merger-driven AGN fueling in detail.

An inevitable consequence of hierarchical clustering of halos (and the eventual merging of their member galaxies) is the formation of systems of multiple BHs. These processes involve several stages that together encompass a huge dynamic range (∼9 orders of magnitude) of separation scales between the BHs. The earliest stages are marked by the gravitational clustering of dark matter halos involving scales ∼1–100 Mpc. The next stage can be marked by when the halos merge and their respective galaxies start interacting; this occurs at scales of ∼100 kpc. The galaxies then eventually merge via dynamical friction (Chandrasekhar 1943). Following the galaxy merger, dynamical friction causes the BHs to continue to inspiral until they reach parsec scales. The timescales for further hardening of the ensuing BH binaries to scales below ∼1 pc are uncertain and may be many Gyr in some cases (Begelman et al. 1980; Milosavljević & Merritt 2003); this is known as the "final parsec problem." Binaries may evolve on these scales via repeated three-body scatterings with stars (Quinlan 1996; Vasiliev et al. 2015; Gualandris et al. 2017; Ogiya et al. 2020) as well as via interactions with gas (Armitage & Natarajan 2002; Sánchez-Salcedo & Chametla 2014; Rafikov 2016). If the binaries reach sufficiently small scales (∼a few megaparsecs), gravitational wave (GW) radiation will take over and cause the BHs to merge; these GWs may be detectable with current and upcoming facilities such as pulsar timing arrays (PTAs) (e.g., Manchester et al. 2013; Desvignes et al. 2016; Verbiest et al. 2016; Ransom et al. 2019) as well as the Laser Interferometer Space Antenna (LISA; Baker et al. 2019). Cosmological hydrodynamic simulations enable us to probe the formation and evolution of such BH systems from ∼1 Mpc to ∼0.01 Mpc scales (the resolution of the simulation prevents us from probing scales smaller than ∼0.01 Mpc). These correspond to relatively early stages of galaxy mergers, which are precursors to gravitational bound BH binaries (BHBs) that will be powerful GW sources for LISA and PTAs. Numerous recent models based on simulations or semi-analytic modeling have made detailed predictions about the formation and evolution of BHBs (Sesana 2010; Khan et al. 2013; Ravi et al. 2014; Holley-Bockelmann & Khan 2015; Bonetti et al. 2016; Kelley et al. 2017; Bonetti et al. 2019; Mannerkoski et al. 2019; Nasim et al. 2020). However, connecting these models to observations continues to be a challenge. Current statistical samples of close BH pairs are largely between ∼1 and 100 kpc scale separations (e.g., Ellison et al. 2011; Liu et al. 2011; Koss et al. 2011; Comerford et al. 2013; Hou et al. 2019; Pfeifle et al. 2019; Hou et al. 2020). In contrast, only one confirmed parsec scale BH *binary* is known (Rodriguez et al. 2006), and the growing population of unresolved, mpc scale binary candidates requires extensive follow-up for confirmation (Liu et al. 2019; Kovačević et al. 2020). Therefore, while these early-stage, ∼1–100 kpc scale BH pairs are still at separations much larger than the GW regime, their properties can serve as an important baseline for BHB models to make predictions on the overall abundances of BHBs and their electromagnetic signatures.

In this work, we use the TNG100 simulation from the IllustrisTNG simulation suite to investigate the possible association between AGN activity and the richness of the AGN environment at a wide range of scales (0.01–1 h^{-1} Mpc). For our purposes, we measure "environmental richness" in terms of BH multiplicity, or the abundance of nearby BHs. In the process, we explore the possibility of enhanced AGN activity associated with multiple BH systems, which (if it exists) may be attributed to a range of physics including (1) large-scale ($\gtrsim$1 h^{-1} Mpc) clustering of massive haloes hosting luminous AGNs and (2) galaxy mergers and interactions on $\lesssim$0.1 h^{-1} Mpc scales producing luminous AGNs. In particular, we identify systems of multiple BHs within separations of 0.01, 0.1, and 1.0 h^{-1} Mpc and investigate the AGN activity of these multiples as compared to that of isolated BHs. We also examine AGN activity in merging BHs, based on the recorded time of BH merger rather than the final pre-merger BH pair separation resolved in the simulation. We do not classify multiple BH systems based on host galaxy properties such as stellar mass ratio (in contrast to the recent study of McAlpine et al. 2020); instead, we focus solely on AGN activity as a function of relative BH positions and merger times. In addition to its simplicity, our approach avoids the uncertainty in measuring stellar masses of close or interacting systems, as tidal stripping tends to strongly alter the mass ratio between first infall and merger (Rodriguez-Gomez et al. 2016; Qu et al. 2017). In addition, our analysis of multiple BH systems on 0.01–1 Mpc scales is complementary to the approach in our companion paper (J. Thomas et al. in preparation), which provides an in-depth analysis of merger-triggered BH growth using higher time resolution BH data. In Section 2, we describe our basic methodology, which includes a brief description of IllustrisTNG, as well as the criteria used for the identification of BH systems. Section 2.4 presents some basic properties of the BH systems, particularly the relationship with their host halos, as well as their abundances. Section 4 focuses on the AGN activity of these BH systems. Section 5 summarizes the main results and conclusions.

2. Methods

2.1. IllustrisTNG Simulation

The IllustrisTNG project (e.g., Marinacci et al. 2018; Nelson et al. 2018; Pillepich et al. 2018a; Nelson et al. 2019; Pillepich et al. 2019) is a suite of large cosmological magnetohydrodynamics (MHD) simulations with three cosmological volumes: TNG50, TNG100, and TNG300, corresponding to box lengths of 50, 100, and 300 h^{-1} Mpc comoving, respectively. The IllustrisTNG simulations are successors to the original Illustris simulation (e.g., Vogelsberger et al. 2014; Nelson et al. 2015), with improved subgrid physics modeling that produces more realistic galaxy populations in better agreement with observations (e.g., Pillepich et al. 2018b;

Springel et al. 2018; Weinberger et al. 2018; Vogelsberger et al. 2020). The simulation was run using the moving mesh code AREPO (Springel 2010; Pakmor et al. 2011, 2016), which solves for self-gravity coupled with MHD. The gravity solver uses the PM-tree method (Barnes & Hut 1986), whereas the fluid dynamics solver uses a finite volume Godunov scheme in which the spatial discretization is performed using an unstructured, moving Voronoi tessellation of the domain. The base cosmology is adopted from the results of Planck Collaboration et al. (2016), which is summarized by the following set of parameters: $\Omega_\Lambda = 0.6911$, $\Omega_m = 0.3089$, $\Omega_b = 0.0486$, $H_0 = 67.74$ km sec^{-1} Mpc^{-1}, $\sigma_8 = 0.8159$, and $n_s = 0.9667$. These cosmological parameters are assumed throughout this work. The simulations were initialized at $z = 127$ using glass initial conditions (White 1994) along with the Zel'dovich approximation (Zel'dovich 1970) to construct the initial displacement field.

Halos are identified using a friends-of-friends algorithm (Davis et al. 1985) with a linking length equal to 0.2 times the mean particle separation. Within these halos, self-bound substructures (subhaloes) are identified using SUBFIND (Springel et al. 2001).

In addition to the gravity and MHD, the simulation includes a wide array of physics to model the key processes responsible for galaxy formation and evolution. Due to resolution limitations, the implementation is carried out in the form of "subgrid" recipes that include the following:

1. Star formation in a multiphase interstellar medium based on the prescription in Springel & Hernquist (2003), with inclusion of chemical enrichment and feedback from supernovae and stellar winds as described in Pillepich et al. (2017).
2. Cooling of metal-enriched gas in the presence of a redshift dependent, spatially uniform, ionizing UV background, with self-shielding in dense gas as described in Vogelsberger et al. (2013).
3. Magnetic fields are included via a small uniform initial seed field ($\sim 10^{-14}$ Gauss) at an arbitrary orientation (Marinacci et al. 2018). The subsequent evolution (coupled with the gas) is driven by the equations of MHD.
4. BH growth via gas accretion and mergers, as well as AGN feedback, which we describe in the following section.

2.2. BH Growth and AGN Feedback in IllustrisTNG

BHs of mass $8 \times 10^5\, M_\odot\, h^{-1}$ are seeded in halos of total mass $> 5 \times 10^{10}\, M_\odot\, h^{-1}$ that do not already contain a BH. Once seeded, these BHs grow via Eddington-limited Bondi–Hoyle accretion given by

$$\dot{M}_{\rm BH} = \max(\dot{M}_{\rm Bondi}, \dot{M}_{\rm Edd}), \tag{1}$$

$$\dot{M}_{\rm Bondi} = \frac{4\pi G^2 M_{\rm BH}^2 \rho}{c_s^3}, \tag{2}$$

$$\dot{M}_{\rm Edd} = \frac{4\pi G M_{\rm BH} m_p}{\epsilon_r \sigma_T} c, \tag{3}$$

where G is the gravitational constant, $M_{\rm BH}$ is the mass of the BH, ρ is the local gas density, c_s is the local sound speed of the gas, m_p is the mass of the proton, ϵ_r is the radiative efficiency, and σ_T is the Thompson scattering cross section. Accreting BHs radiate with a bolometric luminosity given by

$$L = \epsilon_r \dot{M}_{\rm BH} c^2, \tag{4}$$

with an assumed radiative efficiency of $\epsilon_r = 0.2$.

A fraction of the energy released gets coupled to the surrounding gas as thermal or kinetic feedback. IllustrisTNG implements a two-mode feedback model as described in Weinberger et al. (2017), the key features of which are summarized as follows. If the Eddington ratio (defined as $\eta \equiv \dot{M}_{\rm BH}/\dot{M}_{\rm edd}$) exceeds a critical value of $\eta_{\rm crit} = \min[0.002(M_{\rm BH}/10^8 M_\odot)^2, 0.1]$, thermal energy is injected into the neighboring gas at a rate given by $\epsilon_{f,\rm high}\epsilon_r \dot{M}_{\rm BH} c^2$, with $\epsilon_{f,\rm high}\epsilon_r = 0.02$. $\epsilon_{f,\rm high}$ is referred to as the "high accretion state" coupling efficiency. If the Eddington ratio is below this critical value, kinetic energy is injected into the gas at regular intervals of time, in the form of a "wind" oriented along a randomly chosen direction. The injected energy is given by $\epsilon_{f,\rm low}\dot{M}_{\rm BH} c^2$, where $\epsilon_{f,\rm low}$ is referred to as the "low accretion state" coupling efficiency. $\epsilon_{f,\rm low}$ is assigned to have a maximum value of 0.2 with smaller values at very low gas densities. For further details on both feedback modes, we encourage the interested reader to refer to Weinberger et al. (2017).

As with all cosmological-scale simulations, accurate modeling of BH dynamics at small scales is difficult because of the finite simulation resolution. The subgrid BH models used in TNG have been shown to produce reasonable agreement with the observational constraints of the stellar mass—BH mass relations as well as the bright end of the quasar luminosity function, and the AGN feedback prescription is crucial for producing a realistic population of red-and-dead elliptical galaxies (e.g., Weinberger et al. 2017, 2018; Nelson et al. 2018; Pillepich et al. 2018a; Donnari et al. 2019). Thus, while the inherent uncertainty in subgrid models is an important caveat, we see that the TNG models reproduce key empirical constraints on the AGNs and galaxy populations.

Another consideration for modeling BHs in cosmological simulations is the possibility of comparable-mass particles imparting spurious accelerations to the BHs, creating numerical noise. To avoid this, BHs are (re)positioned to the local potential minimum within a sphere containing n neighboring gas cells, where $n = 1000$ is the value assigned for IllustrisTNG. Such a repositioning naturally leads to a prompt merging of two BHs shortly after their parent subhaloes merge. As discussed in detail below, this prompt merging of some black holes limits our ability to study unmerged BH systems on 0.01 h^{-1} Mpc scales. We therefore avoid drawing statistical conclusions about these smallest-scale BH pairs and multiples. This also motivates the inclusion of additional data on merging BH systems in parts of our analysis. All BH merger events, as well as BH accretion rates, are stored as log files during the simulation at much higher time resolution than the simulation snapshots. In Section 4.4, we compare the AGN activity in these merging BHs to that in the small-scale BH pairs identified in simulation snapshots.

2.3. Identifying Systems of BHs

We identify BH systems at various simulation snapshots by linking individual BHs within a maximum distance scale denoted by $d_{\rm max}$. In particular, every member of a BH system must be within a comoving distance $d_{\rm max}$ with respect to at least one other member.

Table 1
Overall Abundances and BH Systems in TNG100 in Terms of Number Densities (in Units of h^3 Mpc^{-3})

z	$n^{\rm bh}$ (h^3 Mpc^{-3})	$d_{\rm max}$ (h^{-1} Mpc)	$f^{\rm sys}(\mathscr{M}=1)$	$f^{\rm sys}(\mathscr{M}=2)$	$f^{\rm sys}(\mathscr{M}=3)$	$f^{\rm sys}(\mathscr{M}=4)$	$f^{\rm sys}(\mathscr{M}>4)$
0	6.01e-02	1.0	25.6%	13.0%	7.77%	5.33%	48.3%
″	″	0.1	88.8%	8.83%	1.75%	0.379%	0.185%
″	″	0.01	99.5%	0.458%	…	…	…
0.6	5.74e-02	1.0	25.5 %	13.9%	8.31%	6.79%	45.5%
″	″	0.1	89.3 %	9.00%	1.38 %	0.314 %	0.0410%
″	″	0.01	99.7 %	0.306%	…	…	…
1.5	4.65e-02	1.0	29.0%	16.0%	9.84%	6.60%	38.5%
″	″	0.1	89.6%	8.78%	1.16%	0.387%	0.0810%
″	″	0.01	99.7%	0.285%	…	…	…
3	1.95e-02	1.0	41.5%	18.1%	10.7%	7.00%	22.7%
″	″	0.1	91.1%	7.88%	0.875%	0.146%	…
″	″	0.01	99.7%	0.267%	…	…	…

Note. $n^{\rm bh}$ (Column 3) is the number density of BHs. $f^{\rm sys}$ (Columns 4–8) is the percentage of BH singles ($\mathscr{M}=1$), pairs ($\mathscr{M}=2$), triples ($\mathscr{M}=3$), quadruples ($\mathscr{M}=4$) and beyond ($\mathscr{M}>4$) at various redshift snapshots (z) and separation scales ($d_{\rm max}$, in comoving h^{-1} Mpc) within the TNG100 simulation box. The percentages (in parentheses) refer to the fraction of BHs living as BH singles, pairs, and multiples.

We investigate systems at three values of $d_{\rm max}$: 1.0, 0.1, and 0.01 h^{-1} Mpc. $d_{\rm max}=1$ h^{-1} Mpc roughly corresponds to typical distances between BHs in halos that have come together via gravitational clustering and are close to a merger; typically, the occupying galaxies themselves are not yet close enough to be visibly interacting. $d_{\rm max}=0.1$ h^{-1} Mpc roughly corresponds to typical distances in the early stages of galaxy interactions, while $d_{\rm max}=0.01$ h^{-1} Mpc corresponds to typical distances in late-stage galaxy mergers. It is important to also note that at the smallest <0.01 h^{-1} Mpc scales, our samples are highly incomplete, because a significant portion of pairs at these scales are promptly merged by the BH repositioning scheme. As discussed below, we find that we are nonetheless able to draw useful qualitative conclusions from the population of unmerged small-scale BH pairs. We additionally perform a more quantitative analysis of BHs in late-stage galaxy mergers (see Appendices B and C) using the complete sample of BH merger progenitors and remnants (which are defined based on merger time, not BH separation). We shall be comparing the results for <0.01 h^{-1} Mpc BH systems to those for the merging BHs, thereby allowing us to identify any systematic bias that may exist within the <0.01 h^{-1} Mpc multiple BH systems due to their incompleteness.

We define *multiplicity* (denoted by $\mathscr{M}$) as the number of members within a BH system. We characterize the AGN activity of a BH system by the member having the highest Eddington ratio; we shall refer to this as the *primary* member of the system. Note that traditionally, the primary is defined to be the most massive BH. However, a merger-triggered enhancement in the AGN activity does not necessarily occur within the most massive member. Therefore, our choice of the highest Eddington ratio member as the primary ensures that within every BH system, we are probing the BHs that are most likely to be associated with merger-triggered AGNs (independent of BH mass). We also note that (unless otherwise stated), our results are qualitatively independent of the choice of the primary (the only exception being in Section 4.4 and is discussed there).

In order to study BH systems on both large and small spatial scales, we need a combination of high enough resolution as well as large enough volume to include a population of rare BH multiples. Therefore, in this work, we use the highest resolution realization of the TNG100 box with 2×1820^3 resolution elements (dark matter particles and gas cells).

2.4. Constructing Randomized Samples of BH Systems

In order to analyze possible sources of selection bias in our results, we prepare an ensemble of "randomized samples" of BH systems. Each randomized sample is constructed by randomly shuffling the "system IDs" (a unique integer ID we assign to each BH that determines which BH system it belongs to, if any) among all the BHs in the simulation. In other words, each system ID is assigned to a random BH within the simulation box. Therefore, for every BH system with multiplicity $\mathscr{M}$, there exists a subset of $\mathscr{M}$ randomly assigned BHs within each randomized sample. Using this procedure, for every sample of BH systems, we constructed an ensemble of 10 corresponding randomized samples that have identical abundances by construction for all multiples (pairs, triples, and beyond).

The following terminology is used for the remainder of the paper. We shall often refer to the actual BH systems within 1, 0.1, and 0.01 h^{-1} Mpc scales as "true systems," and thereby compare their properties to their corresponding "randomized systems"/"randomly selected sets of BHs." Any selection bias in the computation of a quantity for a true system will be fully captured in the trends exhibited by the randomized systems.

3. BH Systems in TNG100

Table 1 summarizes the abundances of the BH systems within the TNG100 box. Here we discuss some of the basic properties (environment and number densities) of these BH systems. Figure 1 shows the multiplicity versus host halo mass of the BH systems identified within the TNG100 universe. Note that for $d_{\rm max}=1$ h^{-1} Mpc, not all members will necessarily be within the same halo; in this case we choose the host halo mass of the

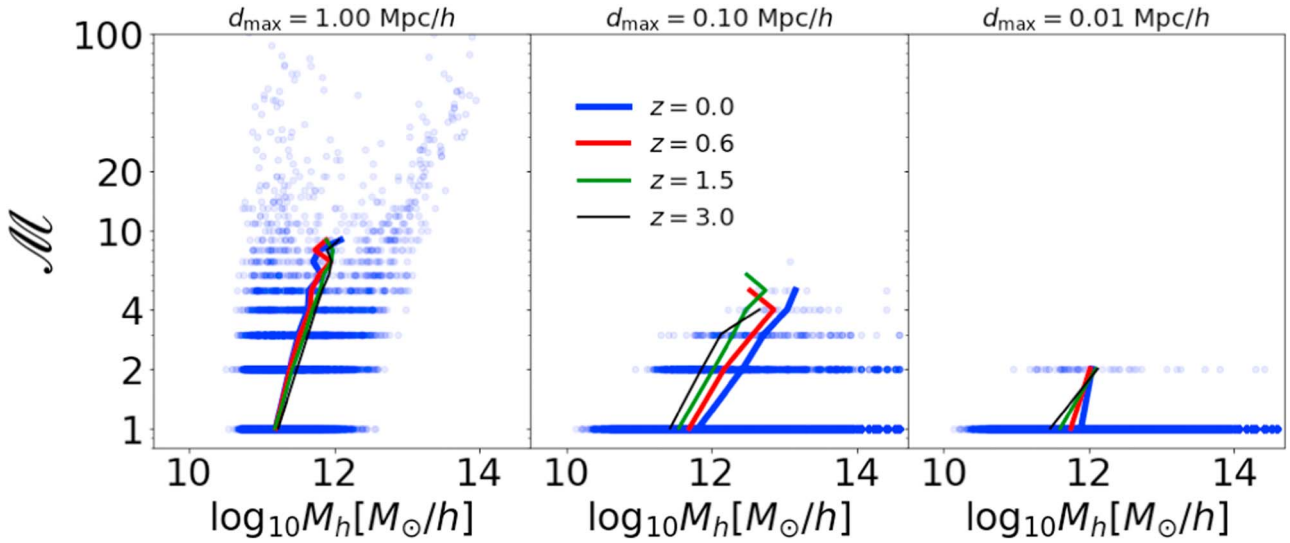

Figure 1. Multiplicity ($\mathscr{M}$) as a function of the host halo mass of the primary BH (member with the highest Eddington ratio), for BH systems (all members have masses $>10^6\ h^{-1}\ M_\odot$) as predicted by the TNG100 simulation. The blue circles correspond to the scatter at $z = 0$. The colored solid lines show the mean trends at $z = 0$, 1.5, 3, and 4. The different panels correspond to different values of d_{max}, which is the maximum comoving distance between a member and at least one other member within the system. We see that more massive halos tend to host richer systems of BHs.

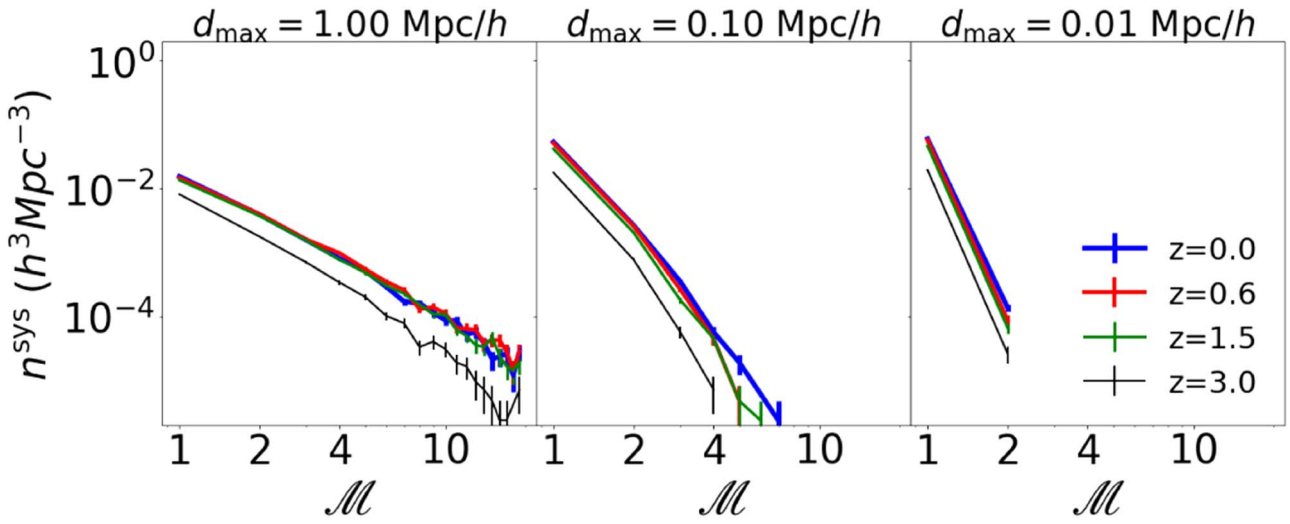

Figure 2. Solid lines show the BH multiplicity functions (defined as the number density n^{sys} of BH systems at each multiplicity $\mathscr{M}$), as predicted by the TNG100 simulation. Horizontal dotted lines mark the overall number density of BHs. Different colors correspond to snapshots at different redshift between $z = 0$ and 3. Left to right panels correspond to $d_{max} = 1$, 0.1, and 0.01 h^{-1} Mpc. The error bars correspond to Poisson errors. The number density of multiple BH systems decreases (roughly as a power law) with increasing multiplicity, and higher-$\mathscr{M}$ BH systems are increasingly rare on small scales (lower d_{max}). Additionally, we also construct 10 randomized samples of BH systems (see Section 2 for how they are constructed) wherein the BHs are randomly grouped together to form systems such that they have the same multiplicity functions as the actual sample.

primary member. Across all scales, we find that systems with higher multiplicity tend to live in more massive halos. This is simply a consequence of higher BH occupations in more massive halos. At scales within 1 h^{-1} Mpc (leftmost panel), BH pairs, triples, and quadruples primarily reside in halos with total mass ranging from $10^{11} - 10^{13}\ h^{-1} M_\odot$, whereas the more massive $M_h \gtrsim 10^{13}\ h^{-1} M_\odot$ halos tend to host BH systems with $\mathscr{M} \gtrsim 10$. The median halo masses ($M_h \sim 10^{11.5-12}\ h^{-1} M_\odot$) of BH systems on these scales vary little with multiplicity. On smaller scales ($\leqslant 0.1\ h^{-1}$ Mpc, middle panel), a stronger trend with M_h is seen; the median halo mass for pairs and triples is $\sim 10^{12}\ h^{-1} M_\odot$, while the highest order multiples at these scales contain up to approximately five members and have median halo masses of $\sim 10^{13}\ h^{-1} M_\odot$. Finally, at scales of $\leqslant 0.01\ h^{-1}$ Mpc (rightmost panel), no higher-order ($\mathscr{M} > 2$) systems are present; BH pairs have median halo masses of $M_h \sim 10^{12}\ h^{-1} M_\odot$.

Now we consider the redshift evolution of the multiplicity versus halo mass relation from $z \sim 0$–3. We focus on scales within 0.1 and 1 h^{-1} Mpc, where there are sufficient statistics for analysis. For BH systems within 0.1 h^{-1} Mpc scales, BH multiples at fixed halo mass are somewhat more common at higher redshift. In part, this reflects the fact that many such systems merge between $z = 3$ and $z = 0$. For 1 h^{-1} Mpc scales, no significant redshift evolution is seen, likely because more of these large-scale BH multiples are still unmerged at $z = 0$.

Figure 2 shows the volume density of the BH systems as a function of multiplicity. At $z = 0$, the number densities for

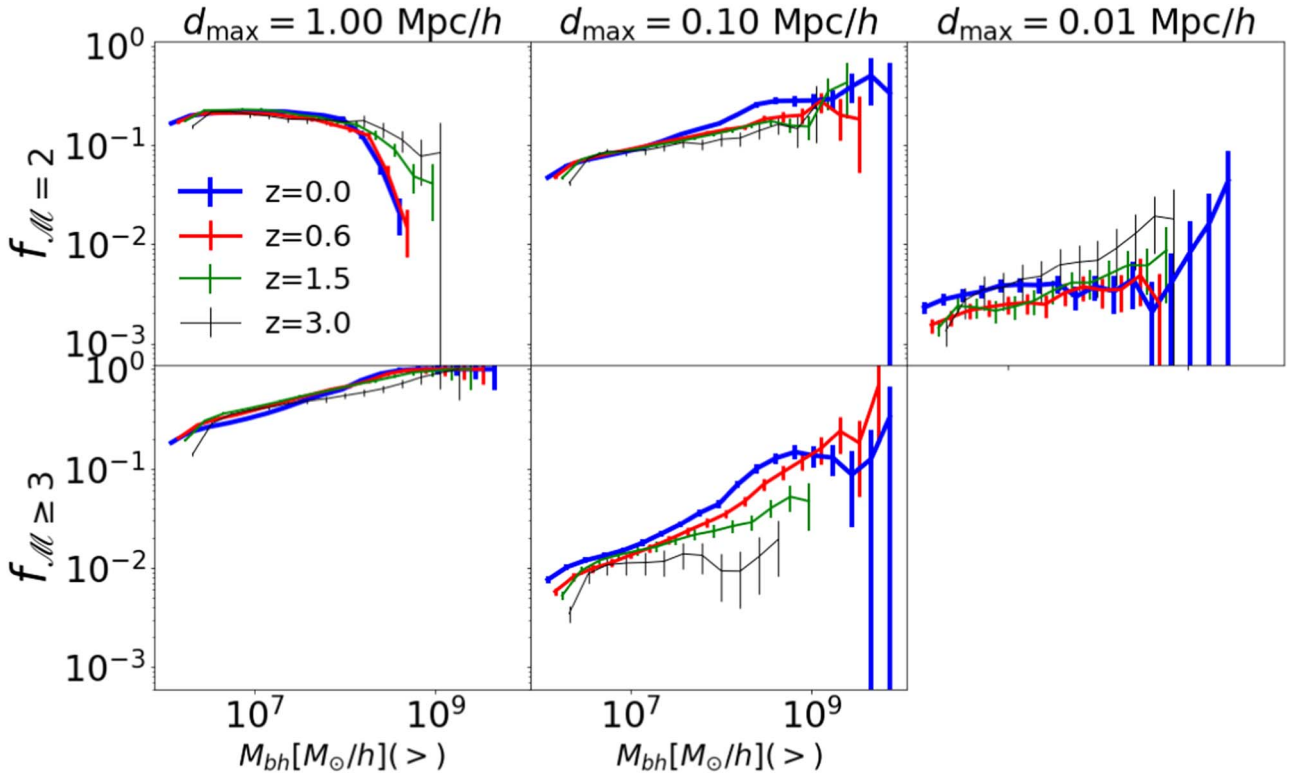

Figure 3. Upper panels: $f_{\mathscr{M}=2}$ is the fraction of systems that are pairs, plotted as a function of BH mass threshold (defined by the mass of the most massive member). Left to right panels correspond to $d_{max} = 1.0$, 0.1, and 0.01 h^{-1} Mpc, respectively. Different colors correspond to snapshots at different redshifts between $z = 0$ and 3. Lower panels: similar to the top panels, but $f_{\mathscr{M}\geqslant 3}$ is the fraction of systems that are triples and higher-order multiples. We find that more massive BHs have a higher likelihood of being members of multiple BH systems.

simulated BH pairs ($\mathscr{M} = 2$) are 3.9×10^{-3}, 2.7×10^{-3}, and $1.4 \times 10^{-4}\,h^3$ Mpc^{-3} at scales of 1.0, 0.1, and 0.01 h^{-1} Mpc, respectively. Comparing this to the number density of the overall BH population at $z = 0$ ($6 \times 10^{-2}\,h^3$ Mpc^{-3}), we see that ∼13% of BHs live in pairs within 1 h^{-1} Mpc scales. At smaller scales ($\leqslant$0.1 and 0.01 h^{-1} Mpc), the percentages of BHs in pairs decrease to ∼9% and ∼0.5%, respectively.

Among the pairs, ∼37% and ∼17% have additional companions to form triples within scales of 1 h^{-1} and 0.1 h^{-1} Mpc, respectively. Some of these systems may eventually form gravitationally bound triple BH systems, which may induce rapid BH mergers and provide a possible solution to the so-called final parsec problem (Bonetti et al. 2016; Ryu et al. 2018). In addition to offering exciting prospects for gravitational wave detections, strong triple BH interactions will often eject the lightest BH from the system, creating a possible population of wandering BHs in galaxy halos (Perets & Alexander 2008; Bellovary et al. 2010).

For higher-order multiples, we see an approximate power-law decrease in the abundance of BH systems with increasing multiplicity for all values of d_{max}. At smaller d_{max}, there are fewer (or no) systems of multiple BHs, which leads to an increasingly sharp decline as we go from $d_{max} = 1\ h^{-1}$ Mpc to 0.01 h^{-1} Mpc. The number densities of BHs and corresponding BH systems are nearly constant at $z < 1.5$, while at $z = 3$ they are lower by a factor of ∼3. For a given value of d_{max}, the relative proportion of BH singles and pairs is nearly constant from $z = 0$–3, and the number density of $\mathscr{M} > 2$ systems at $z = 0$ is only slightly higher (by ∼10% and 60% at $d_{max} = 0.1$ and 0.01 h^{-1} Mpc, respectively) than at $z > 0.6$.

We now focus on how BH multiplicity depends on BH mass. We do this by looking at the relationship between the multiplicity and the most massive member of the system; this is shown in Figure 3 for pairs ($\mathscr{M} = 2$) and multiples ($\mathscr{M} \geqslant 3$). Let us first focus on systems that are exclusively pairs ($\mathscr{M} = 2$). At scales within 0.1 h^{-1} Mpc, the percentage of pairs increases with BH mass from ∼5% for $\sim 10^6\,h^{-1}\,M_\odot$ BHs to ∼20%–40% for $\sim 10^9\,h^{-1}\,M_\odot$ BHs. At scales within 0.01 h^{-1} Mpc, ∼0.2%–2% of BHs live in pairs across the entire range of BH masses; there is some hint of increase in multiplicity with BH mass, although the statistics are very limited. At scales within 1 h^{-1} Mpc, we see that the percentage of pairs remains largely constant at ∼20% up to $\sim 10^8\,h^{-1}\,M_\odot$, and then drops down to $\lesssim$10% at $\sim 10^9\,h^{-1}\,M_\odot$; this is because at these scales, as we increase the mass of BHs, they have a much higher tendency of living in multiples ($\mathscr{M} \geqslant 3$) instead of pairs.

At scales within 0.1 h^{-1} Mpc, the percentage of BHs living in multiples with $\mathscr{M} \geqslant 3$ is ∼1%–2% for $\sim 10^7\,h^{-1}\,M_\odot$ BHs; this increases up to ∼20% for $\sim 10^9\,h^{-1}\,M_\odot$ BHs. At $\leqslant 1\ h^{-1}$ Mpc scales, the percentage increases from ∼30% for $\sim 10^7\,h^{-1}\,M_\odot$ BHs to ∼60% for $\sim 10^8\,h^{-1}\,M_\odot$ BHs; almost all BHs with $\sim 10^9\,M_\odot$ and higher live within 1 h^{-1} Mpc scale pairs. Overall, we find that higher-mass BHs are more likely to have companions, as they live in more massive halos (see Figure 1). Note that this also means that higher multiplicity systems will have higher bolometric luminosities, on average. This motivates our choice (in the following sections) to characterize the luminosity of the BHs in terms of their Eddington ratios; the Eddington ratios do not correlate as strongly with BH mass, making them a better proxy for the probing the AGN activity (independent of the trends seen with BH mass).

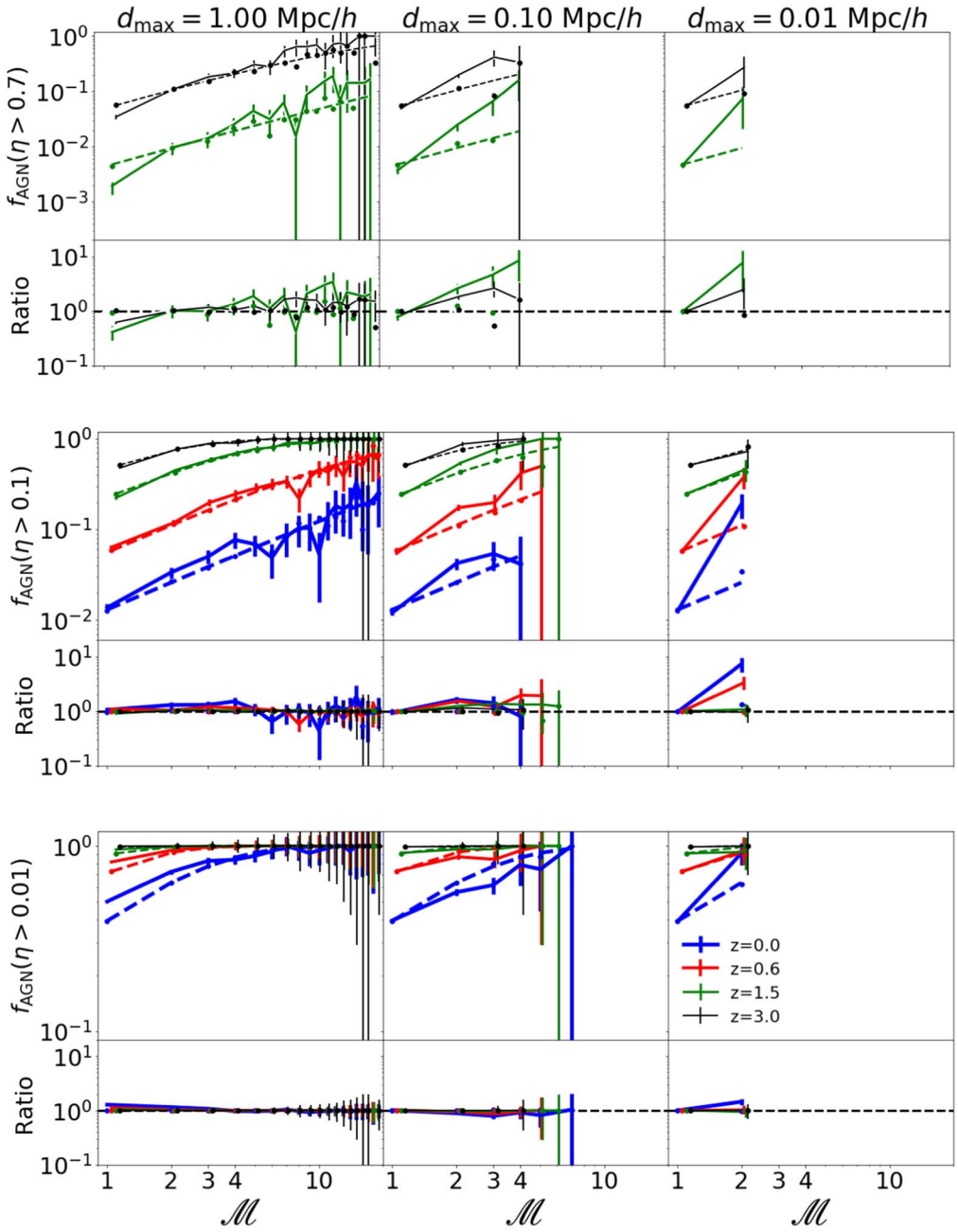

Figure 4. Upper/larger panels: the AGN fraction (f_{AGN}) is defined as the fraction of BH systems that have at least one AGN. Each row assumes a different Eddington ratio threshold to define an AGN, as indicated in the y-axis labels. The solid lines are the AGN fractions for BH systems in `IllustrisTNG`, with error bars corresponding to Poisson errors in their number counts. The filled circles show the median AGN fractions for 10 samples of randomly selected BHs. Additionally, we also have dashed lines that also show predictions for the randomized systems, but computed analytically using Equation (5). As expected, the circles nearly overlap with the dashed lines. The left, middle, and right columns correspond to $d_{max} = 1$, 0.1, and 0.01 h^{-1} Mpc, respectively. Lower/smaller panels: ratios of AGN fractions with respect to analytical predictions for randomly selected BH samples, i.e., the solid lines and filled circles are obtained by comparing the solid lines vs. dashed lines and circles vs. dashed lines, respectively, from the upper panels. At scales within 0.1 and 0.01 h^{-1} Mpc, wherever adequate statistics are available, the highest Eddington ratio of AGNs ($\eta \geqslant 0.1$) are more likely to be found in BH pairs, triples, and higher-order multiples than would be expected from random subsampling. The same is not true at scales of $\leqslant 1$ h^{-1} Mpc, where the higher likelihood for multiple BH systems to contain at least one luminous AGN is mostly a result of simple combinatorics. For low-Eddington ratio thresholds ($\eta > 0.01$), AGN fractions are always high, such that little to no enhancement of AGN activity is detectable in spatially associated BH systems.

4. AGN Activity within BH Systems

4.1. AGN Fractions of BH Systems

Figure 4 shows the fraction (f_{AGN}) of BH systems (as a function of multiplicity) that contain at least one AGN, where "AGNs" are defined via various Eddington ratio thresholds. We see that across the entire range of Eddington ratios and redshifts, systems with higher multiplicity have higher AGN fractions. However, this is to some extent a trivial consequence of the higher probability that a system containing many BHs will contain at least one AGN. In order to quantify the enhancement in AGN activity that can be attributed to environment, we compare this result to AGN fractions (filled circles in Figure 4) of the randomly selected samples of BH

systems (see Section 2.4). Additionally, we can also compute the AGN fractions of the randomized samples analytically (dashed lines in Figure 4). For a sample containing $N_{\rm BH}$ BHs and $N_{\rm AGN}$ AGN, the fraction ($f_{\rm AGN}^{\rm random}$) of randomly chosen sets of $\mathscr{M}$ BHs that have at least one AGN is given by

$$f_{\rm AGN}^{\rm random} = \frac{\binom{N_{\rm BH}}{\mathscr{M}} - \binom{N_{\rm BH}-N_{\rm AGN}}{\mathscr{M}}}{\binom{N_{\rm BH}}{\mathscr{M}}}. \quad (5)$$

We see that the AGN fractions for the randomized samples computed using the two methods (filled circles versus dashed lines) are consistent with each other, providing further validation for our use of randomized samples to identify true enhancements of AGN activity in spatially associated BH systems.

Also evident in Figure 4 is that for BH systems on 1 h^{-1} Mpc scales, there is no significant enhancement of AGN fractions compared to their corresponding randomized samples, even at the highest Eddington ratios ($\eta \geqslant 0.7$). Enhanced AGN fractions are seen for high Eddington ratio AGNs in closer BH systems, however, suggesting a merger-triggered origin for these luminous AGNs. The following describes more details about these enhancements at various Eddington ratio thresholds.

Let us first focus on the AGN fractions of the most luminous AGNs ($\eta \geqslant 0.7$). The topmost panels in Figure 4 contain only data at $z \geqslant 1.5$ (at $z \leqslant 0.6$, the very few $\eta \geqslant 0.7$ AGNs that exist are insufficient to make statistically robust predictions). We see that at scales of 0.1 h^{-1} Mpc, the AGN fractions of BH pairs and multiples ($\mathscr{M} > 1$) are enhanced by up to factors of ∼3–6 compared to their corresponding randomized samples. At the smallest ($\leqslant$0.01 h^{-1} Mpc) scales, we see hints of a similar trend, but there are too few luminous AGN systems to draw definite conclusions. In contrast, BHs that are isolated ($\mathscr{M} = 1$) at 1 h^{-1} Mpc scales are actually slightly *less* likely to host luminous AGNs than individual BHs sampled randomly from the overall population. These trends imply a strong association between luminous AGN triggering and BH multiplicity on $\leqslant$0.1 h^{-1} Mpc scales.

If the AGN Eddington ratio threshold is decreased to $\eta_{\rm min} = 0.1$, enhanced AGN fractions are seen for $d_{\rm max} \leqslant 0.1$ Mpc systems at all redshifts (excepting $z = 3$, where most primary BHs are $\eta \geqslant 0.1$ AGNs even in the randomized samples). These AGN enhancements are smaller (up to factors ∼2) than those for the most luminous AGNs ($\eta > 0.7$) at $\leqslant$0.1 h^{-1} Mpc scales. On the smallest ($\leqslant$0.01 h^{-1} Mpc) scales, however, the AGN fractions of BH pairs at low redshift are more strongly enhanced (up to factors of ∼8 at $z = 0$) compared to their corresponding randomized pairs.

If the AGN Eddington ratio threshold is further decreased to $\eta_{\rm min} = 0.01$, no significantly enhanced AGN fractions are seen in any multiple BH systems. A notable exception is $\leqslant$0.01 h^{-1} Mpc scale pairs at $z = 0$, which are enhanced by up to factors of ∼2.

In a nutshell, the above trends indicate that AGNs are more likely to be found in multiple BH systems at (1) high Eddington ratios and (2) smaller BH separations. Because multiple BH systems on $\leqslant$0.1 h^{-1} Mpc scales are likely to be hosted in ongoing galaxy interactions or mergers, this finding is in agreement with previous studies indicating enhanced AGN activity in interacting galaxies (Liu et al. 2011; Silverman et al. 2011; Ellison et al. 2011, 2013; Lackner et al. 2014; Satyapal et al. 2014; Weston et al. 2017; Goulding et al. 2018; Ellison et al. 2019). Our findings are also in agreement with previous studies suggesting that luminous AGNs are strongly clustered in rich environments at small scales $\lesssim$0.1 h^{-1} Mpc, in particular the "one-halo" term of the AGN/quasar clustering measurements (Kayo & Oguri 2012; Eftekharzadeh et al. 2017). Finally, the fact that no enhancements are seen at 1 h^{-1} Mpc scales is also consistent with previous clustering studies, which find no significant luminosity dependence on large-scale clustering amplitude (Li et al. 2006; Krumpe et al. 2018; Wang & Li 2019; Powell et al. 2020).

4.2. What Fraction of Observable AGNs Are Members of BH Systems?

As mentioned earlier, some observational studies also look for "merger fractions" of AGNs—i.e., what fraction of AGNs are hosted by merging/interacting systems. In terms of our work, a robust proxy for these merger fractions is the fraction of AGNs that are members of BH pairs and multiples. Figure 5 (solid lines) shows the fraction ($f_{\mathscr{M}\geqslant}$) of primary AGNs that are members of BH systems of a threshold multiplicity $\mathscr{M}\geqslant$, plotted as a function of threshold Eddington ratio $\eta_{\rm min}$. These are compared to corresponding predictions for AGNs belonging to the randomized samples. We find that in the regime of Eddington ratio thresholds between ∼0.01 and 1, higher Eddington ratio AGNs are more likely to have one or more companions compared to lower Eddington ratio AGNs. However, this trend is also seen for the randomized samples, which shows that this is (in part) due to our choice of the most luminous member as the primary; this accompanies an inherent statistical bias in favor of more luminous AGNs being more likely to be picked out from higher-order BH systems. For $\eta < 0.01$, $f(\mathscr{M}\geqslant)$ tends to gradually flatten for both randomized samples and true samples, but this is simply because as we continue to decrease the Eddington ratio threshold, we eventually cover the full AGN population. If we look at the redshift evolution at a fixed Eddington ratio threshold, we see that lower-redshift AGNs have a higher probability of being a member of a BH multiple. This is primarily because at fixed multiplicity, BH systems tend to have decreasing Eddington ratios at lower redshifts due to a general decrease in AGN luminosity with decreasing redshift (as seen in Appendix A, Figure 12); as a natural corollary, at fixed Eddington ratio, BH systems have higher multiplicities at lower redshifts.

We now look at the difference in the $f(\mathscr{M}\geqslant)$ between the true samples of BH systems and the corresponding randomized samples in order to filter out the effects that are physical (see ratio plots of Figure 5). At scales of 1 h^{-1} Mpc, we see no significant difference between $f(\mathscr{M}\geqslant)$ predictions for the true samples and the randomized samples for the entire range of Eddington ratio thresholds; this is similar to our findings for the AGN fractions in the previous section. As we approach scales of 0.1 h^{-1} Mpc, we find that $f(\mathscr{M}\geqslant)$ is enhanced for the true samples as compared to the randomized samples at high enough Eddington ratios. These enhancements start to appear at $\eta \sim 0.01$ and increases up to factors of ∼4 for the most luminous AGNs ($\eta \sim 0.7$–1). At scales within 0.01 h^{-1} Mpc, we see the strongest enhancements; in particular, if we look at $z = 0$, 0.6 pairs where we have the best statistics, the enhancements are up to factors of ∼7–9 for the most luminous AGNs ($\eta \sim 0.1$). Furthermore, at $z = 0$ the enhancements start appearing at Eddington ratios as low as $\eta \gtrsim 0.001$.

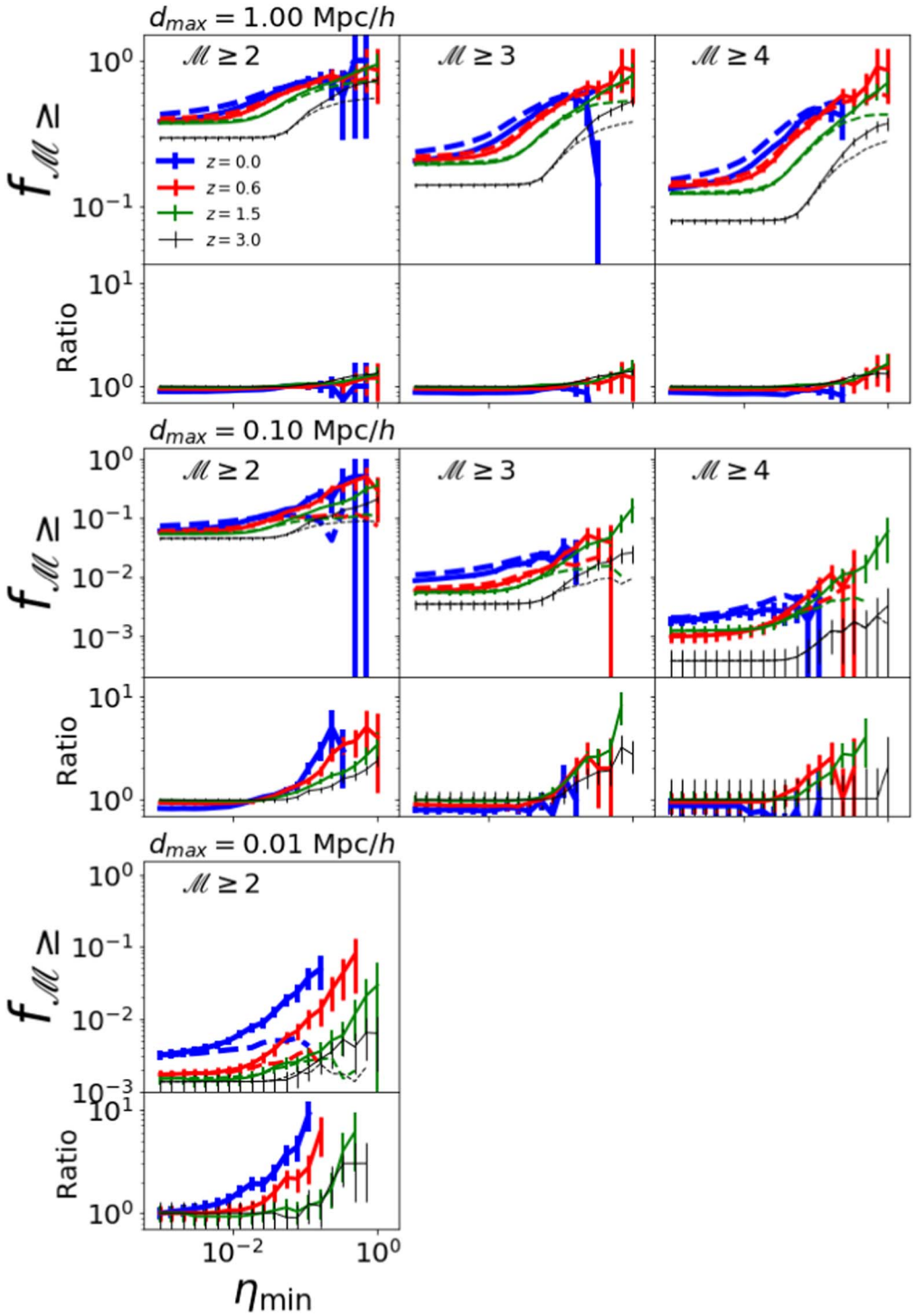

Figure 5. Upper/larger panels: $f_{\mathscr{M}(\geqslant)}$ refers to the fraction of primary AGNs that live in BH systems with a minimum multiplicity $\mathscr{M}(\geqslant)$; this is plotted as a function of the threshold Eddington ratio $\eta_{\rm min}$. Solid lines correspond to the BH systems, and dashed lines correspond to the median values for the 10 samples of randomly selected BHs. The top, middle, and bottom rows correspond to $d_{\rm max} = 1$, 0.1, and 0.01 h^{-1} Mpc, respectively. The error bars correspond to Poisson errors. Within each row, the lower/smaller panels denote the ratio (solid/dashed lines) between the predictions for the true BH systems vs. that of the randomized systems. The left, middle, and right panels correspond to systems with at least two, three, and four members, respectively. The different colors correspond to different redshifts. At higher Eddington ratios, the likelihood of an AGN belonging to multiple BH systems within 0.1 and 0.01 h^{-1} Mpc scales is significantly enhanced compared to that of the randomized systems; on the other hand, there is very little enhancement for BH systems within 1 h^{-1} Mpc scales.

To summarize the above trends, we find that more luminous AGNs have an enhanced likelihood of having companion BHs within 0.1 h^{-1} Mpc; at the same time, there is no enhancement in the likelihood of AGNs having companion BHs within 1 h^{-1} Mpc. This further corroborates the inferences drawn in the previous sections, i.e., no signatures of large-scale AGN clustering are seen in our identified BH systems, but enhanced AGN activity is associated with rich environments at small scales ($\leqslant$0.1 h^{-1} Mpc), likely triggered by mergers and interactions between galaxies.

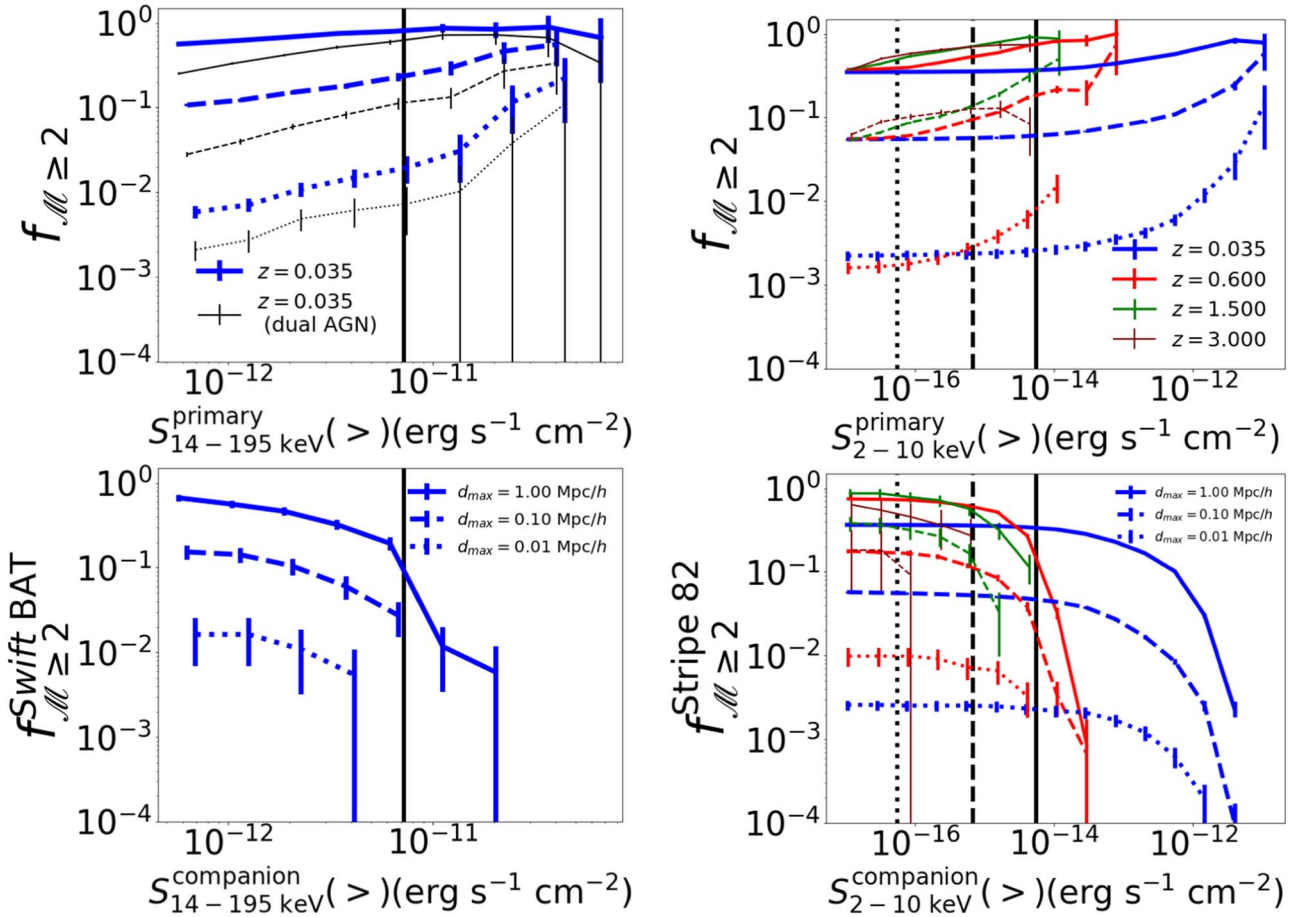

Figure 6. Upper panels: the fraction $f(\mathscr{M} \geqslant 2)$ of primary AGNs (defined here to be the most luminous member of the BH system) with 14–195 keV (right panel) and 2–10 keV (left panel) threshold flux, that live in pairs/multiples. The different colors generally correspond to different redshifts (see legend). In the left panel, the thin black lines correspond to systems where the companion BHs have $L_{2-10\,\rm keV} > 10^{42}$ erg s^{-1} at $z = 0.035$. Solid, dashed, and dotted lines correspond to $d_{\rm max} = 1$, 0.1, and 0.01 h^{-1} Mpc, respectively. The assumed bolometric corrections for the X-ray bands have been adopted from Vasudevan et al. (2010) (left panel) and Lusso et al. (2012) (right panel). The vertical line in the right panel marks the detection limit (7.2×10^{-12} erg s^{-1} cm^{-2}) for the 105 month Swift-BAT survey (Oh et al. 2018). The vertical lines in the left panel mark detection limits of the following fields obtained from the Chandra X-ray observatory: the dotted line (5.5×10^{-17} erg s^{-1} cm^{-2}) corresponds to the Chandra Deep Fields-North and South (CDF-N and CDF-S); the dashed line (6.7×10^{-16} erg s^{-1} cm^{-2}) corresponds to the Extended Chandra Deep Field—South (ECDF-S); and the solid line (5.4×10^{-15} erg s^{-1} cm^{-2}) corresponds to the Chandra Stripe 82 ACX survey (LaMassa et al. 2013). At the detection threshold of Swift-BAT, the fraction of ultra-hard X-ray AGNs associated with BH pairs and multiples within scales of 0.1 h^{-1} Mpc is ∼10%–20%. At the Stripe 82 ACX detection limit, the fraction of hard X-ray AGNs in 0.1h^{-1} Mpc scale pairs and multiples is ∼10%–20% (5%) at $z \sim 0.6$–1.5 (at $z \sim 0.035$). Lower panels: $f^{\rm Swift\ BAT}_{\mathscr{M}\geqslant 2}$ ($f^{\rm Stripe\ 82}_{\mathscr{M}\geqslant 2}$) is defined as the fraction of Swift-BAT (Stripe 82) primary AGNs that have at least one detectable companion above a given flux threshold (x-axes show the flux threshold of the companion AGNs). ∼3% of Swift-BAT AGNs at $z = 0.035$ have companions within 0.1 h^{-1} Mpc that are detectable at the 105 month survey limit.

4.2.1. Companions of X-Ray Selected AGNs

From an observational perspective, it is also instructive to estimate the fraction of AGNs in BH pairs and multiples that would be detectable in a survey with a given flux limit. Therefore, in addition to analyzing AGN samples characterized by Eddington ratios, we now repeat our analysis by characterizing AGNs in multiple BH systems based on their estimated intrinsic fluxes in the 2–10 keV (hard) and 14–195 keV (Swift-Burst Alert Telescope (BAT) ultra-hard) X-ray bands (Figure 6, upper panels). For the 2–10 keV band, the bolometric corrections are adopted from Lusso et al. (2012), where they assumed best-fit relations between the bolometric luminosities and 2–10 keV X-ray luminosities of the AGN samples from the XMM-Cosmological Evolution Survey a.k.a COSMOS (Cappelluti et al. 2009) survey. For the 14–195 keV X-ray band, we assume a constant bolometric correction of 15, as in previous analyses of Swift-BAT AGNs (e.g., Vasudevan et al. 2010; Koss et al. 2012). Figure 6 (upper panels) shows the fraction of AGNs found in multiple BH systems ($f_{\mathscr{M}\geqslant 2}$) as a function of the assumed hard or ultra-hard X-ray flux threshold. We see that in either case, brighter AGNs are more likely to live in pairs and multiples, which is not surprising given the trends seen with Eddington ratios.

We first focus on predictions for ultra-hard X-ray AGNs (Figure 6, left panels). The 105 month all-sky Swift-BAT survey has a flux limit of 7.2×10^{-12} erg s^{-1} cm^{-2} in the 14–195 keV band (Oh et al. 2018). At these X-ray energies, even heavily obscured AGNs experience little attenuation. Coupled with its sky coverage, this means that the Swift-BAT survey yields a uniquely complete sample of low-redshift AGNs ($z \lesssim 0.05$). We present predictions for the simulation snapshot at $z = 0.035$ (blue lines in Figure 6, upper-left panels). Let us first look at 1 h^{-1} Mpc scales, where we previously found no enhanced AGN activity in BH pairs or multiples. We see that the majority (∼70%–80%) of the detectable AGNs live in BH pairs and multiples within scales

of 1 h^{-1} Mpc. In line with our previous results, however, we conclude that this is primarily driven by the gravitational clustering of halos hosting BHs and has little to do with the AGN activity of the BHs. On scales $\leqslant 0.1\ h^{-1}$ Mpc, where we did previously find enhanced AGN activity in multiple BH systems, we see that ∼10%–20% of the detectable AGN population is associated with BH pairs and multiples.

We can compare this population to the Swift-BAT-selected AGN sample studied in Koss et al. (2012). Using optical imaging, they selected BAT AGNs hosted in galaxies that have companions within 100 projected kpc. Koss et al. (2012) then compared with 2–10 keV X-ray observations to identify those companions that also hosted AGNs to determine the dual AGN frequency on these scales. They assumed a minimum AGN luminosity of $L_{2-10\,\mathrm{kev}} > 10^{42}$ erg s^{-1}, to avoid confusion with X-ray emission from star-forming regions. We apply similar criteria to identify dual AGNs in our data, selecting AGNs that would be detectable in the 105 month BAT survey and that have companion AGNs within 0.1 h^{-1} Mpc with $L_{2-10\,\mathrm{kev}} > 10^{42}$ erg s^{-1}. Using these criteria, we find that ∼10% of BAT-detected AGNs in our sample are dual AGNs on 0.1 h^{-1} Mpc scales (black-dashed lines in Figure 6, upper-left panel). This is consistent with the results of Koss et al. (2012).

In the lower left panel of Figure 6, we examine the fraction of BAT AGNs with at least one companion BH that would also be detected at the limit of the BAT survey. The fraction decreases with increasing flux, owing to the rarity of luminous AGNs. We see that at $z \sim 0.035$, ∼3% and ∼10% of BAT AGNs have companions within 0.1 and 1 h^{-1} Mpc, respectively, that are detectable at the 105 month survey limit.

We similarly examine the companions of hard X-ray selected AGNs, based on their inferred intrinsic 2–10 keV flux. We do not attempt to model the amount of AGN obscuration, although we note that many AGNs have significant attenuation in the 2–10 keV band, particularly in late-stage mergers (e.g., Kocevski et al. 2015; Ricci et al. 2017; Secrest et al. 2020). These results will therefore be most useful for comparison with X-ray AGNs for which intrinsic luminosities can be estimated. We focus on the Chandra Stripe 82 ACX survey (solid vertical line in Figure 6), owing to its large area (∼17 deg^2) that yields statistically large samples of X-ray bright AGNs. At 1 h^{-1} Mpc scales (due to gravitational clustering), ∼70%–80% of the detectable AGNs live in BH pairs and multiples at $z \sim 0.6$–3; this decreases to ∼40% at $z \sim 0.035$. At $\leqslant 0.1\ h^{-1}$ Mpc scales, ∼10%–20% of the detectable AGN population is associated with BH pairs and multiples at $z \sim 0.6$–1.5; this decreases to ∼5% at $z \sim 0.035$. Within 0.01 h^{-1} Mpc scales, $\lesssim$1% of the detectable AGNs are associated with BH pairs.

These findings are consistent with our previous results; for the Eddington ratio selected AGNs in Figure 5, we see that at the highest Eddington ratios, only up to ∼40% of AGNs have companions within 0.1 h^{-1} Mpc. Overall, this suggests that the majority of AGN activity is actually *not* associated with mergers/interactions, but is instead driven by secular processes. This agrees with other recent observational (Villforth et al. 2014, 2017; Marian et al. 2019; Zhao et al. 2019) and theoretical studies (McAlpine et al. 2020).

Finally, we examine the fraction of Stripe 82 AGNs that would have companions detectable at various flux limits, giving rise to dual or multiple AGNs (lower right panel of Figure 6). Here we primarily focus on summarizing the results for companions within $\leqslant 0.1\ h^{-1}$ Mpc (where we report statistically robust evidence of AGN enhancements), but results at $\leqslant 0.01{,}1\ h^{-1}$ Mpc are also presented in Figure 6 for completeness. At $z \sim 0.035$, where the Stripe 82 flux limit corresponds to an AGN luminosity of $\sim 3 \times 10^{40}$ erg s^{-1}, almost all the available companions are detectable, implying that ∼5% of Stripe 82 AGNs have companions already detectable without deeper observations. However, such low luminosities are quite difficult to distinguish from X-ray emission from star-forming regions. At $z \sim 0.6$, where even intensely star-forming regions are unlikely to mimic detectable AGNs at the Stripe 82 limit, ∼2% of Stripe 82 AGNs have companions detectable without deeper observations. At higher redshifts ($z \sim 1.5{,}3$), there are no companions that are detectable within Stripe 82. However, the prospect of detecting companions is better for deeper observations such as the Chandra Deep Field (CDF) and extended Chandra Deep Field (ECDF) surveys. In particular, at the flux limit of the ECDF, almost all the available companions are detectable, implying that ∼20% and ∼30% of Stripe 82 AGNs at $z = 1.5$ and $z = 3$, respectively, have companions detectable at the ECDF limit.

4.3. Disentangling AGN Enhancements in Multiples from Trends with Host Mass

We have so far established that there is enhanced AGN activity in close systems of multiple BHs ($\leqslant 0.1\ h^{-1}$ Mpc). The AGN enhancement at these scales may partly be attributed to AGNs triggering by galaxy mergers and interactions. At the same time, there may also be a contribution from: (1) a possible correlation between the AGN Eddington ratio and the mass of its host halo or galaxy, and (2) the fact that more massive haloes host a higher number of galaxies containing BHs, and therefore are richer in both active and inactive BHs. In this section, we shall statistically control for the host halo and galaxy mass and further look for possible enhancements in the AGN activity within BH systems that can be solely attributed to small-scale galactic dynamics.

Figure 7 shows the Eddington ratio versus the BH mass of the overall BH populations within TNG100. We first divide the population based on whether the luminosities are higher (orange histograms) or lower (green histograms) than the median Eddington ratio at fixed BH mass. We then ensure that for each of the two populations, we select subsamples with similar host halo masses and host galaxy stellar masses, using the following procedure. In Figure 8, orange and green solid lines show the resulting host halo mass functions of the BH samples represented by histograms of the corresponding color in Figure 7. The sharp drop in the halo mass function at $M_h \sim 5 \times 10^{10}\ h^{-1}\ M_\odot$ corresponds to the threshold halo mass for inserting BH seeds. (The small tail of $M_h < 5 \times 10^{10}\ h^{-1}\ M_\odot$ halos correspond to those that have seeded BHs at an earlier time, but have lost some mass due to tidal stripping.) We find that for halos with $M_h \gtrsim 10^{12}\ h^{-1}\ M_\odot$ and $M_h \lesssim 10^{11}\ h^{-1}\ M_\odot$, the halo mass functions for hosts of high- and low-Eddington ratio BHs differ slightly in their normalization. Thus, for this analysis we focus on BHs hosted in $10^{11} < M_h < 10^{12}\ h^{-1}\ M_\odot$ halos at all snapshots between $0 < z < 4$, where the difference in the halo mass function is small ($\lesssim$30%).

We follow the same procedure for host galaxy stellar masses (M_*), wherein we select galaxies with $10^{8.6} < M_* < 10^{10.6}\ h^{-1}\ M_\odot$ such that the stellar mass functions differ by $\lesssim$30% between high- and low-Eddington ratio BH hosts (Figure 9: blue regions). Overall, we have (1) divided the BH

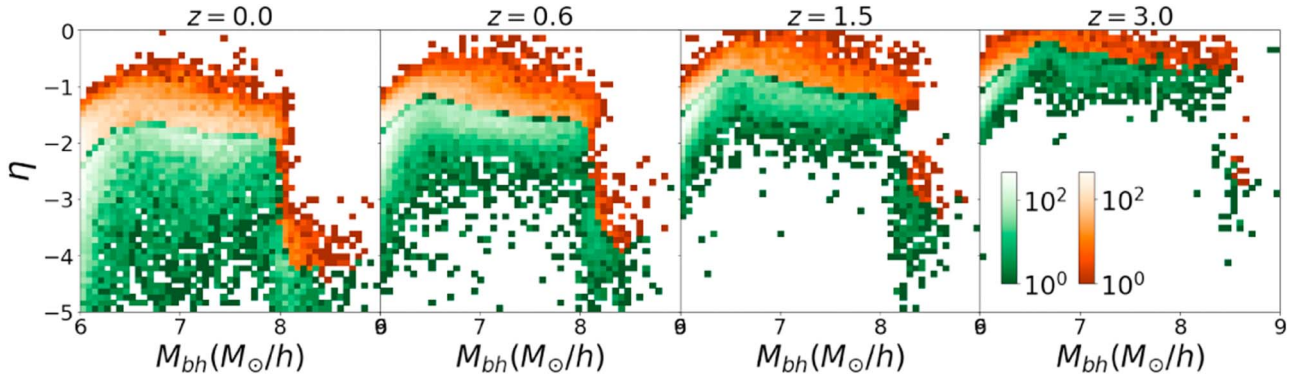

Figure 7. AGN Eddington ratio (η) vs. BH mass ($M_{\rm bh}$). The overall sample is split into objects with Eddington ratios higher (orange histograms) and lower (green histograms) than the median Eddington ratio at fixed BH mass. From left to right, the panels show snapshots at $z = 0$, 0.6, 1.5, and 3. This demonstrates how we split the BHs into high- and low-Eddington ratio populations to investigate the relative likelihood of these populations to live in BH pairs and multiples.

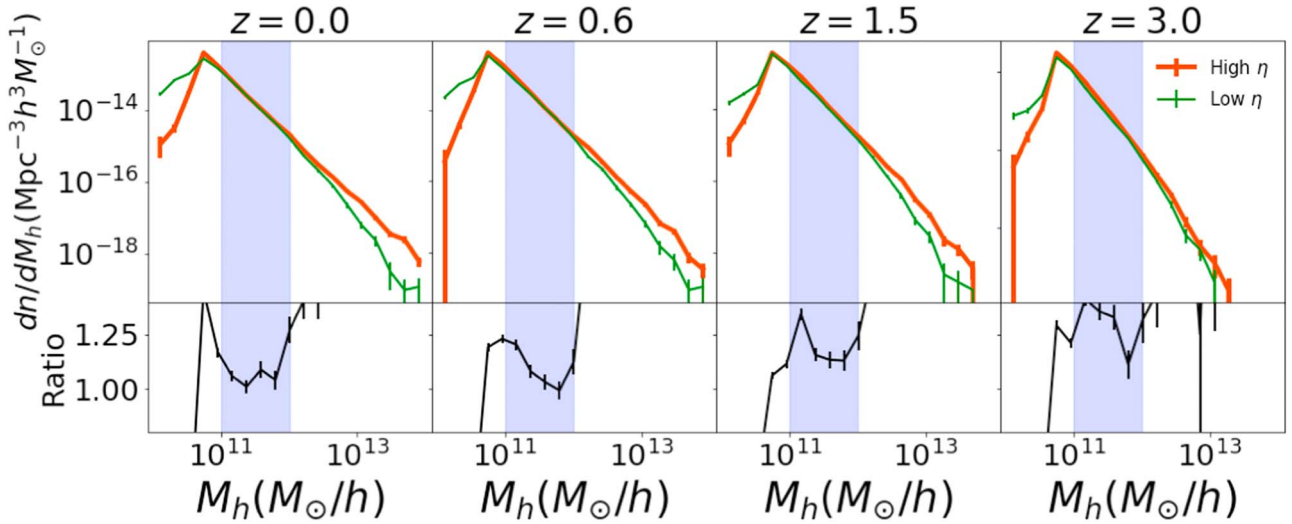

Figure 8. Top panels: orange and green solid lines are the host halo mass (M_h) functions of BHs with Eddington ratios higher and lower than the median value at fixed BH mass. Bottom panels: ratio between the orange vs. green lines presented on the top panels. The blue region ($10^{11} < M_h < 10^{12}\,h^{-1}\,M_\odot$) represents the BHs that were selected for the computation of $f(\mathscr{M}\geqslant)$ in Figure 10. This region is chosen to ensure that the halo mass functions for the high- and low-Eddington ratio populations of Figure 7 match to within ∼30%. From left to right, the panels show snapshots at $z =$ 0, 0.6, 1.5, and 3.

population into those with Eddington ratios higher and lower than the median value at fixed BH mass, and (2) further selected subsamples of both the populations with minimal differences in their host halo masses and host galaxy stellar masses. In the process, we have constructed two BH subsamples with similar host halo properties that differ solely in their Eddington ratios. We can now quantify the fraction of AGNs in each of these subsamples that live in BH pairs and multiples, relative to the corresponding randomized BH samples.

Figure 10 (upper panels) shows the fraction $f(\mathscr{M} \geqslant 2)$ of AGNs that are primary members of BH pairs and multiples, plotted as a function of redshift for the high- and low-Eddington ratio populations of primary BHs described above (and in Figures 7–9). The solid and dashed lines correspond to the predictions for the true BH systems and the randomized samples, respectively. For both the randomized samples as well as true samples, more luminous AGNs have a greater likelihood of being members of BH systems, compared to those that are less luminous. This, again, is in part due to the statistical bias arising due to our choice of the most luminous AGNs as the primary. In order to isolate the physical effects, we look at the ratio of $f(\mathscr{M} \geqslant 2)$ between the true samples and the randomized samples, which are shown in Figure 10 (lower panels). At scales within 0.1 h^{-1} Mpc, we find that (with the exception of $z \sim 0$) the likelihood for more luminous AGNs to live in BH pairs and multiples is enhanced for the true samples compared to that of randomized samples. Likewise, the likelihood of less luminous AGNs to live in BH pairs and multiples is suppressed for the true samples compared to that of randomized samples. Therefore, at $z \gtrsim 0.6$, we see clear evidence that at scales of $\leqslant 0.1\ h^{-1}$ Mpc, BH pairs and multiples are indeed associated with more enhanced AGN activity, independent of the overall masses of the host halos and galaxies.

At $z \sim 0$, we do not see any enhancement at $\leqslant 0.1\ h^{-1}$ Mpc scales. This is simply because the typical Eddington ratios at $z = 0$ are lower overall (median Eddington ratio ∼0.01, see Figure 7). As we saw in Figure 5, no significant enhancements are seen in low-luminosity ($\eta \lesssim 0.01$) AGNs for $d_{\rm max} \geqslant 0.1$ h^{-1} Mpc BH systems. However, if we look at $\leqslant 0.01\ h^{-1}$ Mpc scales, we do see evidence of enhanced AGN activity at $z \lesssim 2$, including at $z = 0$.

Additionally, note that the enhancements in $f(\mathscr{M} \geqslant 2)$ seen in Figure 10 are significantly smaller than the strongest enhancements reported for the most luminous AGNs ($\eta \gtrsim 0.7$)

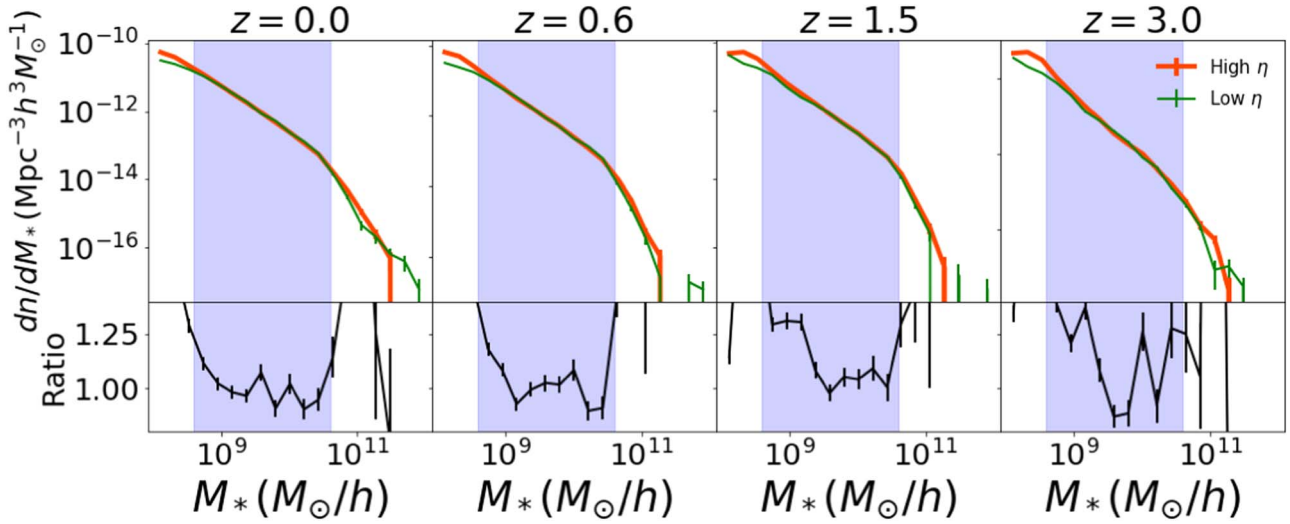

Figure 9. Top panels: orange and green solid lines are the host galaxy (subhalo) stellar mass (M_*) functions of BHs with Eddington ratios higher and lower than the median value at fixed BH mass. Bottom panels: ratio between the orange vs. green lines presented on the top panels. The blue region represents the BHs that were selected for the computation of $f(\mathscr{M} \geqslant)$ in Figure 10. This region of $10^{8.6} < M_h < 10^{10.6}\,h^{-1}\,M_\odot$ is chosen to ensure that the stellar mass functions for the high- and low-Eddington ratio populations of Figure 7 match to within ∼30%. From left to right, the panels show snapshots at $z =$ 0, 0.6, 1.5, and 3.

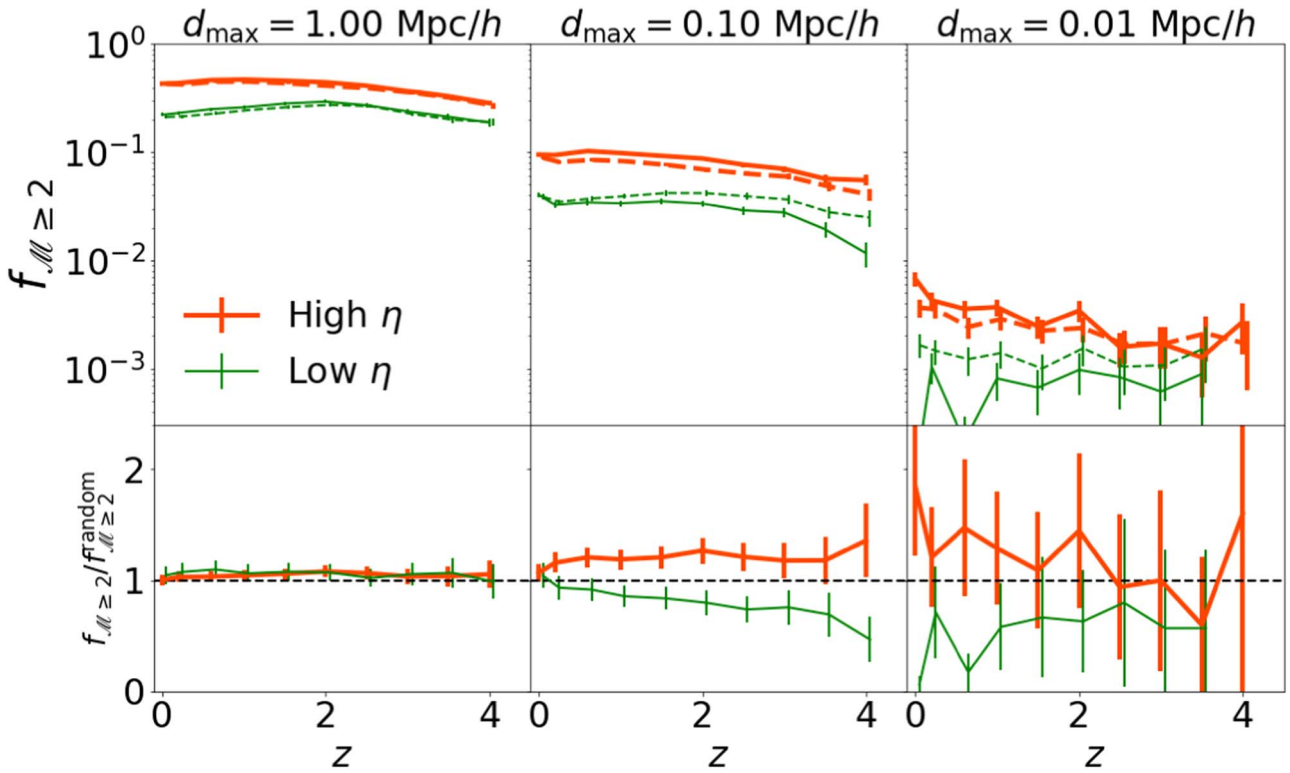

Figure 10. Upper/larger panels: $f(\mathscr{M} \geqslant 2)$ as a function of redshift is the fraction of primary AGNs that live in pairs. The orange and green lines represent primary AGNs with Eddington ratios higher and lower, respectively, than the median value at fixed BH mass. The solid lines correspond to true BH systems, while the dashed lines correspond to the median values of 10 randomized systems. We further subsample the populations such that host halo and stellar masses are confined to the green highlighted regions in Figures 8 and 9, respectively. Lower/smaller panels: the ratio between the predictions of $f(\mathscr{M} \geqslant)$ for the true samples of BH systems vs. that of the randomized samples. We find that the high Eddington ratio primary AGNs (orange lines) have *slightly higher likelihood* of belonging to multiple BH systems within scales of 0.1 and 0.01 h^{-1} Mpc, compared to random subsets of BHs. At the same time, low-Eddington ratio primary AGNs (green lines) have *slightly lower likelihood* of belonging to a multiple BH systems at scales within 0.1 and 0.01 h^{-1} Mpc, compared to randomly chosen subsets of BHs. These effects are not seen at scales of 1 h^{-1} Mpc.

shown in Figure 5. But this is simply because selecting the high Eddington ratio samples in Figure 10 is broadly equivalent to samples with "effective Eddington ratio thresholds" ranging from $\eta \sim 0.01$ at $z = 0$ to $\eta \sim 0.1$ at $z = 3$ (see Figure 7); these values are significantly smaller than $\eta \gtrsim 0.7$ and therefore correspond to weaker enhancements. Lastly, we also show the results for the $\leqslant 1$ h^{-1} Mpc scale multiples (leftmost panels in Figure 10), wherein we find no difference in $f(\mathscr{M} \geqslant 2)$ between true and randomized BH systems; this is expected, given the results in Figure 5.

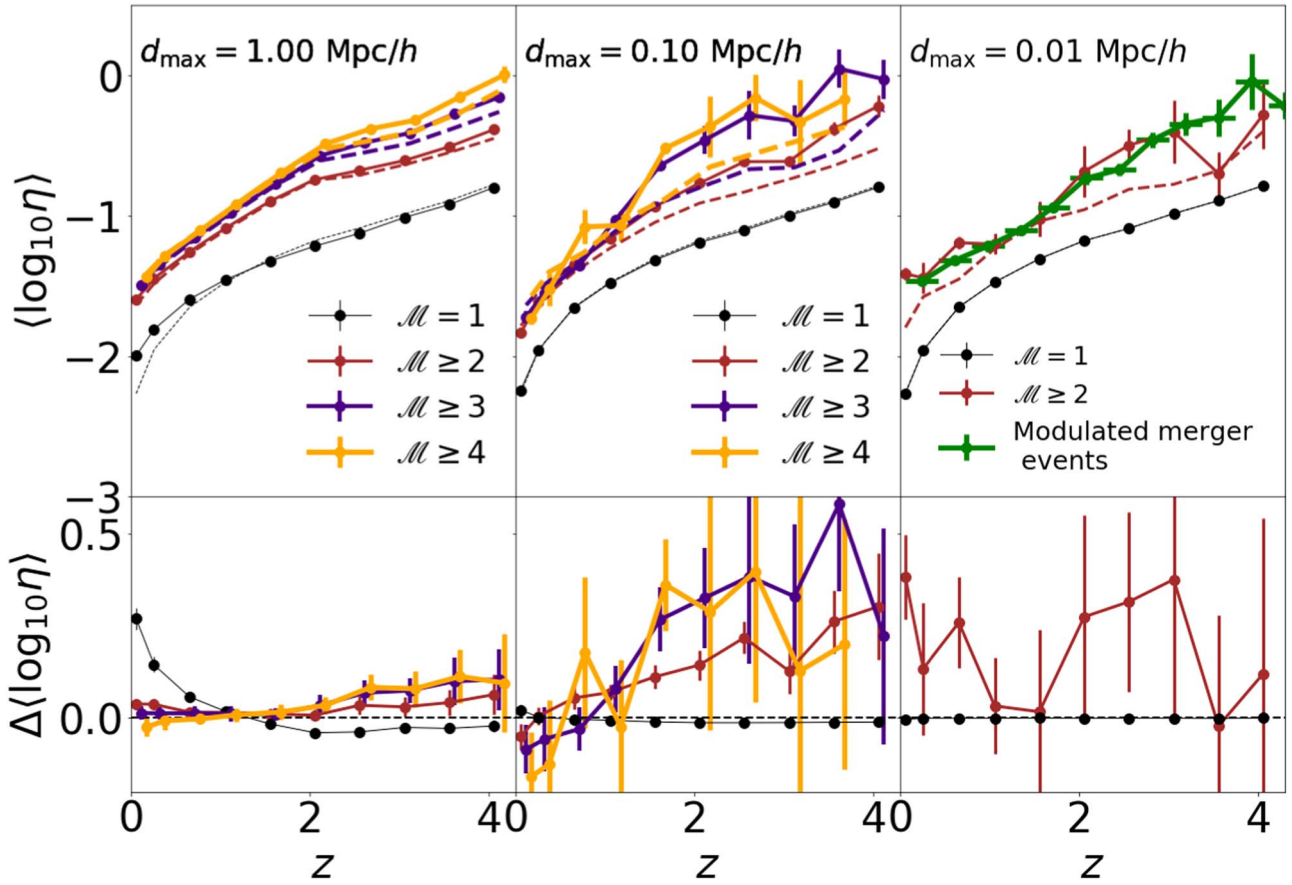

Figure 11. Upper /larger panels: median values of the AGN Eddington ratio $\langle \log_{10}\eta \rangle$ of the primary BHs of pairs and multiples as a function of redshift. The maroon, purple, and orange circles correspond to all multiple BH systems with $\mathscr{M} \geqslant 2$, 3, and 4, respectively. The black circles correspond to isolated BHs ($\mathscr{M} = 1$). The dashed lines correspond to the median values for 10 samples of randomly selected systems. The green lines correspond to pairs of merging BHs recorded at high time resolution during the simulation run; the sample of merging BHs has been modulated to have similar distributions of masses and mass ratios as the 0.01 h^{-1} Mpc pairs. Lower, smaller panels: the difference (solid-dashed lines) between $\langle \log_{10}\eta \rangle$ for the true BH systems vs. the randomized systems. The different rows correspond to various values of d_{max}. The error bars on the y-axis are obtained using bootstrap resampling. We see that Eddington ratios associated with primary BHs are enhanced when they belong to BH systems on 0.1 or 0.01 h^{-1} Mpc scales, relative to randomly chosen subsets of BHs. On 0.01 h^{-1} Mpc scales, the AGN enhancements are most significant at $z \sim 0$. In contrast, little enhancement in AGN activity is seen in BH systems at scales of 1 h^{-1} Mpc.

To summarize, the results in this section further solidify the association of enhanced AGN activity with BH pairs and multiples within scales of 0.1 h^{-1} Mpc. When controlled for host halo mass, the fraction of high Eddington ratio AGNs that are in multiple BH systems is only modestly enhanced over random associations. Nonetheless, our results demonstrate that this trend does exist independent of the fact that massive halos and galaxies tend to host more luminous and more numerous BHs. This enhancement in AGN activity is likely driven by mergers and interactions between galaxies.

4.4. Impact of a Small-scale Environment on the Eddington Ratios of BH Systems

Having established the influence of a small-scale ($\leqslant 0.1$ h^{-1} Mpc) environment on AGN activity, we now quantify in greater detail the magnitude of Eddington ratio enhancements in BH pairs and multiples compared to isolated BH. In particular, we look at the Eddington ratios associated with the primary members of BH multiples ($\mathscr{M} \geqslant 2$, 3, 4) as well as those of isolated BHs ($\mathscr{M} = 1$), as a function of redshift. Figure 11 shows that the Eddington ratios for the true sample of BH multiples increase with multiplicity at fixed redshift, but so do the Eddington ratios of the random samples. This again is due to the fact that the primary AGNs form a biased sample compared to the full population.

We are most interested in the comparison of the median Eddington ratios between the true samples of BH multiples and the randomized samples (solid versus dashed lines); these are shown in the lower panels of Figure 11. At scales of 1 h^{-1} Mpc, the median Eddington ratios for the true samples of BH multiples have minimal differences ($\lesssim$0.1 dex) with respect to the randomized samples, as expected from our analysis so far. At scales of $d_{max} = 0.1$ h^{-1} Mpc (middle panel), we find that the Eddington ratios for the true samples of BH multiples tend to be increasingly enhanced at higher redshifts. At the highest redshifts of $z \sim$ 3–4, the enhancements are up to ~0.3–0.5 dex. This agrees with our results in Figure 10 and likely reflects stronger enhancements in merger-driven AGN activity due to greater availability of cold gas at higher redshifts. At the lowest redshifts of $z \lesssim 0.6$, there is no significant enhancement of the Eddington ratios at $\leqslant 0.1$ h^{-1} Mpc scales.

At separation scales of $d_{max} = 0.01$ h^{-1} Mpc, however, where we only have BH pairs, we find that at $z \lesssim 0.6$, the median Eddington ratios for the true samples are enhanced by ~0.3–0.4 dex. (At higher redshifts, some evidence of enhanced Eddington ratios is also seen, but the results are at best only marginally significant.) As we discussed earlier, our sample of

BH pairs at these scales is incomplete, because a significant fraction of them merge prematurely due to the BH repositioning scheme implemented by the simulation. Therefore, we simultaneously look at the complete sample of BH mergers. These events are recorded in log files at every time step of the simulation, and are therefore stored at a much higher time resolution than the snapshot data. There are 24,048 merger events recorded during the simulation run. In Appendix B, we look for possible bias that can arise due to this incompleteness, and find that the primary source of bias is the mass ratio of the merging BHs. In particular, the mass ratios of $<0.01\ h^{-1}$ Mpc pairs is significantly higher than that of the merger sample (see Appendix B for more details). We therefore modulate the sample of merging BHs such that it has similar distributions of mass ratios as the sample of $0.01\ h^{-1}$ Mpc BH pairs. We perform the modulation based on randomly selecting subsamples of BHs at various bins of mass ratios and masses, where the relative fraction of objects in each bin is tuned to represent the mass ratio and mass distributions of $0.01\ h^{-1}$ Mpc BH pairs (we do this to make the samples more comparable, since the Eddington ratios have been found to depend on the mass ratios as well as masses of the merging BHs). After the modulation we end up with 1970 merging BH systems (as compared to the much smaller number of $0.01\ h^{-1}$ Mpc scale BH pairs, which is only 285). We find that the median Eddington ratios of these merging BH pairs (cyan lines in the rightmost panel) are broadly consistent with that of the $0.01\ h^{-1}$ Mpc scale pairs. In addition, we also find similar Eddington ratio enhancements for the full sample of merger remnants, details of which are shown in Appendix C. Thus, the results for the sample of $0.01\ h^{-1}$ Mpc scale pairs as well as the merger events reflect an enhancement of AGN activity associated with small separations.

To summarize, we find a measurable impact of the small-scale ($\leqslant 0.1\ h^{-1}$ Mpc) environment on AGN Eddington ratios, which generally tends to increase at higher redshift. The median Eddington ratios are, at best, enhanced up to factors of $\sim$2–3 (0.3–0.5 dex). This supports the existence of a merger-AGN connection. However, because the enhancements in AGN activity for BH pairs and multiples are relatively modest, our results do not suggest that merger-driven AGN fueling is a dominant channel of BH growth overall (see also McAlpine et al. 2020, and J. Thomas et al. 2020, in preparation).

5. Conclusions

In this work, we investigate the role of environment on AGN activity within the TNG100 realization of the IllustrisTNG simulation suite. In particular, we investigate whether BH pairs and multiples (within separations of 0.01–1 h^{-1} Mpc) have enhanced AGN activity compared to samples of randomly assigned pairs and multiples.

The number density of BHs in TNG100 is $n \sim 0.06\,h^3$ Mpc^{-3} at $z \lesssim 1.5$ ($n \sim 0.02\,h^3$ Mpc^{-3} at $z = 3$). About 10% of these BHs live in pairs on scales of $0.1\ h^{-1}$ Mpc, and $\sim$10% of these pairs (i.e., $\sim$1% of all BHs) have additional companions, forming triples or higher-order multiples. A similar fraction ($\sim$12%) of BHs are in pairs on $1\ h^{-1}$ Mpc scales, but $\sim$30% of these ($\sim$3.6% of all BHs) have additional companions on these scales. On the smallest scales ($d_{\rm max} = 0.01\ h^{-1}$ Mpc), in contrast, only $\sim$0.2% of BHs are found in pairs (though as discussed above, this sample of pairs is incomplete). Overall, pairs and triples live in halos with a range of masses, but the median host halo mass ($\lesssim 10^{12}\,h^{-1}\,M_\odot$) varies little with redshift.

We find that the AGN activity associated with these BH systems is enhanced at scales within $0.01\ h^{-1}$ Mpc and $0.1\ h^{-1}$ Mpc across the entire redshift regime ($z \sim$ 0–4) we covered in this study. However, no such enhancements are found for BH systems within 1 Mpc scales. The lack of enhancements in AGN activity at $\sim$1 Mpc scales, is consistent with recent observational constraints on large-scale clustering, which were found to exhibit no significant dependence on AGN luminosity. On the other hand, the enhancements at smaller scales $\sim$0.01 and $0.1\ h^{-1}$ Mpc can be attributed to AGN activity triggered by merging and interacting galaxies.

The influence of the small-scale ($\leqslant 0.1\ h^{-1}$ Mpc) environment on the AGN activity is strongest at high Eddington ratios. In particular, for the highest Eddington ratio ($\gtrsim$0.7) AGNs, the AGN fractions are significantly enhanced (up to factors of $\sim$3–6) for pairs, triples, and quadruples at scales within $\leqslant 0.1\ h^{-1}$ Mpc compared to random BH samples. As we decrease the Eddington ratio thresholds, these environmental enhancements gradually become smaller and eventually disappear around Eddington ratios of $\sim$0.01. Additionally, the enhancements (at fixed Eddington ratio) also tend to be highest at the smallest ($\leqslant 0.01\ h^{-1}$ Mpc) scales. We note again the caveat that subgrid BH models introduce uncertainty into our results. However, the good agreement between observed AGNs and galaxy populations and those in TNG suggests that these uncertainties do not dominate our results. In particular, we undertake a more careful analysis of possible impacts of the BH repositioning scheme on our conclusions. Recall that the sample of $\leqslant 0.01\ h^{-1}$ Mpc pairs is incomplete, because the BH repositioning scheme causes many such systems to promptly merge. However, we illustrate in Appendices B and C that our conclusions do not depend on this issue, and that qualitatively similar results are found for the full sample of BH mergers. For example, at Eddington ratios greater than 0.1, the AGN fractions of $\leqslant 0.01\ h^{-1}$ Mpc pairs at $z = 0$ are enhanced up to factors of $\sim$8. Similarly, we also find that more luminous AGNs have an enhanced likelihood (up to factors of $\sim$4 and $\sim$9 within 0.1 and $0.01\ h^{-1}$ Mpc scales, respectively) of living in BH pairs and multiples, compared to random subsamples of BHs.

In order to control for possible systematic biases, we investigate whether our results are influenced by the possibility that more luminous AGNs tend to live in more massive galaxies and halos, which incidentally tend to also host a higher number of BHs. We found that even after statistically controlling for the host halo mass and host galaxy stellar mass, more luminous AGNs continue to have enhanced likelihood of living in BH pairs and multiples within $0.1\ h^{-1}$ Mpc, compared to random subsamples of BHs. This further solidifies the correlation between AGN activity and the richness of the small-scale ($\leqslant 0.1\ h^{-1}$ Mpc) environment over the entire redshift range between 0 and 4. Additionally, we find that the enhancement in accretion rates within BH systems is stronger at higher redshift, which presumably reflects the higher cold gas fractions at higher redshifts.

Because the Eddington ratio of AGNs is not a directly observable quantity (and BH mass measurements must often rely on indirect methods), we also estimate the X-ray luminosities of the AGNs in our sample and determine the likelihood for X-ray selected AGNs to live in BH pairs and multiples, as a function of the X-ray flux limits relevant to

current surveys. At the limit of the 105 month Swift-BAT survey, about ∼10%–20% of detectable AGNs at $z = 0.035$ have at least one secondary companion within 0.1 h^{-1} Mpc scales. ∼3% of these BAT AGNs have companions that are also detectable at the Swift-BAT survey flux limit. Additionally, when we define dual AGNs as in Koss et al. (2012) (i.e., when AGN companions are selected based on a minimum 2–10 keV luminosity of 10^{42} erg s^{-1}), we report a dual AGN frequency of ∼10%, consistent with their measurements.

If instead we consider the companions of AGNs selected in the 2–10 keV band at the limit of the Chandra Stripe 82 survey (with no constraints on the ultra-hard X-ray band), we find that ∼5% of AGNs live in pairs and multiples within 0.1 h^{-1} Mpc scales at $z = 0.035$. At higher redshifts ($z \sim 0.6$–1.5), up to ∼30% of such AGNs have companions within 0.1 h^{-1} Mpc scales. However, for only $\lesssim$2% of these $z \gtrsim 0.6$ AGNs, the companions are detectable without observations deeper than Stripe 82. At the flux limits of ECDF, most of the companions (up to $z \sim 3$) are available for detection, but those with low X-ray luminosities will likely be indistinguishable from star formation, and many will also have significant dust attenuation.

With its wide-field imaging capabilities, the upcoming Advanced Telescope for High Energy Astrophysics (Athena) mission (Barret et al. 2013) will enable new surveys that are expected to detect hundreds of AGNs at $z > 6$ (Nandra et al. 2013). The proposed Advanced X-ray Imaging Satellite (Mushotzky 2018) and Lynx X-ray Observatory (Lynx) missions (The Lynx Team 2018) would enable detection of large new populations of AGNs, including high redshift AGNs and close ($\lesssim$0.01 h^{-1} Mpc) dual AGNs, owing to their subarcsecond imaging requirements and their factors of 10 and 100, respectively, better sensitivity than Chandra. Our finding that merger-driven AGN activity is a significant but subdominant channel for BH fueling in TNG100 provides additional motivation for pursuing these key science goals with Athena.

While the enhanced AGN activity in rich, small-scale environments is consistent with the presence of the merger-AGN connection, we find that only a subdominant (at best ∼40% for the highest Eddington ratio AGNs) fraction of AGNs actually live in BH pairs and multiples. Furthermore, enhancements in the Eddington ratios in BH pairs and multiples are, at best, only up to factors ∼2–3. Therefore, most AGN fueling as well as BH growth in TNG100 may still be primarily triggered by secular processes, with a significant but minor role played by galaxy mergers/interactions. We plan to explore these questions in more detail in future work, including our companion paper, J. Thomas et al. (2020, in preparation).

L.B. acknowledges support from National Science Foundation grant AST-1715413.

Appendix A
Scaling Relation between Eddington Ratio versus Multiplicity of BH Systems

Here, we briefly discuss the overall scaling relation between Eddington ratio versus BH multiplicity, which is shown in Figure 12. We see that BH systems having higher Eddington ratios (for the primary member) have higher multiplicities at all scales between 0.01 and 1 h^{-1} Mpc. The correlation tends to be somewhat stronger at smaller separation scales, particularly at $z \sim 0$, 0.6. The redshift evolution tells us that BH systems at all multiplicities tend to have lower Eddington ratios (at fixed $\mathscr{M}$) at lower redshifts, which is due to the general decrease in the AGN luminosity with decreasing redshift at $z \lesssim$ 2–3. Conversely, this also implies that BH systems of a given Eddington ratio tend to have higher multiplicities at lower redshifts.

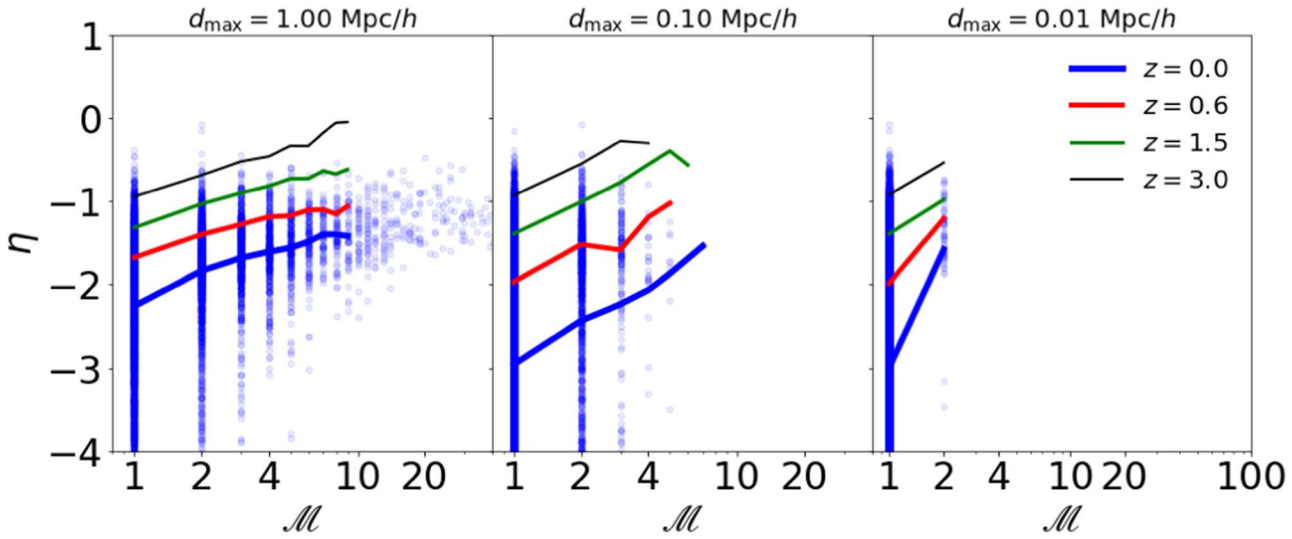

Figure 12. Eddington ratio (η) as a function of the multiplicity ($\mathscr{M}$) of the primary BH (member with the highest Eddington ratio), for BH systems as predicted by the TNG100 simulation. The blue circles correspond to the scatter at $z = 0$. The solid lines are the median relations at various redshifts. We see a positive correlation between the BH multiplicity and the Eddington ratio of the primary member, which tends to be stronger at smaller scales (particularly at $z = 0$,0.6). The redshift evolution shows that at fixed multiplicity, Eddington ratios decrease with decreasing redshifts; conversely, at fixed Eddington ratio, BH systems have higher multiplicities at lower redshifts.

Appendix B
Imcompleteness of 0.01 h^{-1} Mpc Scale Pair Sample

Our sample of $<0.01\ h^{-1}$ Mpc pairs is incomplete due to the "prompt" BH mergers that ensue from the BH repositioning scheme implemented in the simulations. Here, we explore the possible biases that can occur in our analysis due to the incompleteness. To do this, we compare statistics of our $<0.01\ h^{-1}$ Mpc pair sample to that of the complete set of merger events recorded during the simulation. For the purpose of this and the next section (Appendices B and C), we shall go back to the conventional scheme of referring to the more massive merging BH as the "primary"; the less massive merging BH is referred to as the "secondary". Figure 13 (upper panels) shows the distributions of primary (more massive) and secondary (less massive) BHs. We find that the mass ratios of the $<0.01\ h^{-1}$ Mpc pairs (black lines) are significantly higher compared to the complete sample of mergers (red lines). This difference is largely coming from the primary BHs, which have significantly smaller masses for the $<0.01\ h^{-1}$ Mpc pairs as compared to the merger events, whereas the secondary BH mass distributions are similar for both the samples. This is expected as the lower mass primaries tend to live in shallower potentials, leading to a longer time to merge with the secondary; this increases the likelihood of the pairs with lower mass primaries to appear in a snapshot before they merge. We then modulate the merger sample, so as to have similar mass ratio distribution as that of the $<0.01\ h^{-1}$ Mpc pairs; we refer to this as the sample of "modulated merger events" (shown as green lines in Figure 13). More specifically, the modulation is performed by subsampling the merger events at bins of different mass ratios, based on the fraction of $<0.01\ h^{-1}$ Mpc scale pairs that belong to that bin.

We now investigate the gas, stellar, and dark matter mass content associated with the environments of the $<0.01\ h^{-1}$ Mpc pairs and compare them with that of the complete sample of merger events. Figure 13 (lower panels) shows the distributions of the gas, stellar, and dark matter masses (within the stellar half mass–radius $R_{1/2}$) of the progenitor subhaloes at the closest snapshot prior to merger. The gas mass distributions for the merger events (red lines) are slightly broader than those of the $<0.01\ h^{-1}$ Mpc pairs (black lines). However, the peaks of both distributions are at similar mass ($2 \times 10^9 M_\odot/h$), implying that $<0.01\ h^{-1}$ Mpc pairs do not have a significantly higher gas content to fuel mergers compared to the full sample of merger events. The stellar masses for the merger events are significantly higher than those of the $<0.01\ h^{-1}$ Mpc pairs, this (as discussed in the next paragraph) is due to the higher primary BH masses in the merger events, and the correlation between BH mass and subhalo stellar mass. Lastly, the dark matter masses are peaked at similar values ($\sim 10^{10} M_\odot/h$) for both the $<0.01\ h^{-1}$ Mpc pairs and the merger events; however, the distribution for the merger events has a high mass tail between $\sim 10^{11} - 10^{13} M_\odot/h$, which is completely absent for the $<0.01\ h^{-1}$ Mpc pairs.

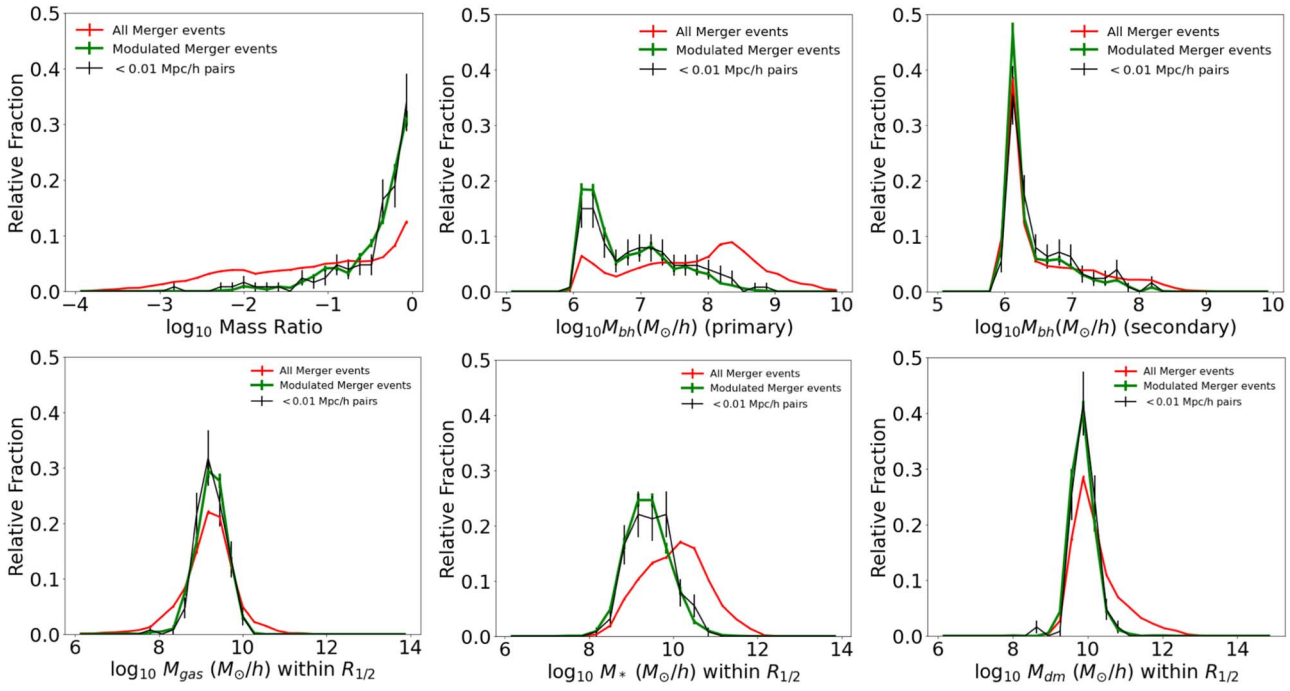

Figure 13. Upper panels: the leftmost panels show distributions of the mass ratios between primary (more massive) and secondary (less massive) BHs. The middle and right panels show the primary and secondary BH masses, respectively. We compare the distributions for $<0.01\ h^{-1}$ Mpc scale pairs (black lines) vs. the complete set of BH merger events (red lines). The mass ratios of the $<0.01\ h^{-1}$ Mpc scale pairs are significantly skewed toward higher values compared to that of the full set of merger events; this is largely due to the primary BH masses being smaller for the $<0.01\ h^{-1}$ Mpc scale pairs compared to the merger events. We therefore modulate the merger events to have the same mass ratio distribution as the $<0.01\ h^{-1}$ Mpc scale pairs. We do this by subsampling the merger events at bins of different mass ratios, based on the fraction of $<0.01\ h^{-1}$ Mpc scale pairs that belong to each bin. The modulated sample of merger events are shown as the green lines. Lower panels: the distributions of the gas mass, stellar mass, and dark matter mass (within the stellar half mass radii) of the progenitor galaxies (subhaloes) found within the snapshot immediately prior to the merger. If the primary and secondary BHs have different progenitor subhaloes, their masses are added together. The line colors are the same as in the upper panel (see legend). For the merger events, the distribution of gas mass is slightly broader than that of the $<0.01\ h^{-1}$ Mpc scale pairs, but they both peak at similar values ($2 \times 10^9 M_\odot/h$). The stellar mass distribution for the $<0.01\ h^{-1}$ Mpc scale pairs is skewed toward smaller values compared to the merger events. Lastly, Overall, the distribution of modulated merger events is similar to that of the $<0.01\ h^{-1}$ Mpc scale pairs, implying that the biases in the progenitor masses are predominantly driven by the bias in the mass ratios seen in the upper panel.

We now assess what fraction of the bias seen in the environment (gas, stellar, and dark matter masses) of the <0.01 h^{-1} Mpc pairs, is driven by the bias in mass ratios. To do this, we compare the gas, stellar, and dark matter mass distributions for the <0.01 h^{-1} Mpc pairs against the modulated merger events (black lines versus green lines in Figure 13, lower panels). We find that upon enforcing the mass ratio distributions for the modulated merger events to be similar to that of <0.01 h^{-1} Mpc pairs, the distributions of gas, stellar, and dark matter masses also become similar for the two samples. This establishes that the bias seen within the <0.01 h^{-1} Mpc pairs is primarily dominated by the difference in mass ratio distributions of the two samples. Therefore, in addition to presenting Eddington ratios for the <0.01 h^{-1} Mpc pairs in Section 4.4, we also present the results for the modulated merger events with mass ratios similar to that of the <0.01 h^{-1} Mpc pairs; we show that both these samples have similar Eddington ratios. For further completeness, we also look at the AGN activity of the full sample of merger events in Appendix C.

Appendix C
AGN Activity in Merger Remnants

In Appendix B, we have seen how the BH pairs at <0.01 h^{-1} Mpc scales are incomplete and have biased environmental properties compared to the full sample of merging BHs in TNG100. We demonstrated that this bias can be attributed to the difference in mass ratio distributions between the two populations. For completeness, here we look at the AGN activity of the entire population of merger remnants. Figure 14 (upper panels) shows the median Eddington ratios of merger remnants (black lines) at each snapshot of TNG100; we first compare this to the median Eddington ratios for the full population of BHs (blue lines). We find that for $z \gtrsim 2$, the Eddington ratios of merger remnants are enhanced compared to the full BH population (left to right panels); these enhancements tend to increase with increasing redshifts up to $z \sim 5$ (for $z > 5$, the merger remnants accrete at the Eddington limit). Additionally, the Eddington ratios of merger remnants are not sensitive to mass ratio thresholds (left to right panels) at $z \gtrsim 2$. At $z \lesssim 2$, we find that the Eddington ratios of merger remnants start to become significantly sensitive to the mass ratios. For mass ratio threshold of 10^{-4} (leftmost panel), we find that the merger remnants have suppressed Eddington ratios compared to the full BH population. As we increase the mass ratio threshold, the Eddington ratios of merger remnants increase, and eventually become similar to that of the full BH population for mass ratio thresholds of 10^{-1} (rightmost panel). The reason why the inclusion of the lowest mass ratio (10^{-4} to 10^{-3}) mergers suppresses the Eddington ratios at low redshift is that their primary BHs have masses $>10^9\,M_\odot/h$. For these BHs, the kinetic mode of AGN feedback drives outflows of gas and suppresses gas accretion. The foregoing motivates us to further compare the Eddington ratios of merger remnants to populations of BHs with similar mass. In particular, at each snapshot, we modulated the full BH population to form BH samples that have similar BH mass distributions as those of the merger remnants. We refer to the resulting BH subpopulations as "modulated BH samples" (shown as red lines in Figure 14, upper panels). The difference in the Eddington ratios of the merger remnants compared to the modulated BH samples is shown in the lower panels. We find that merger remnants have

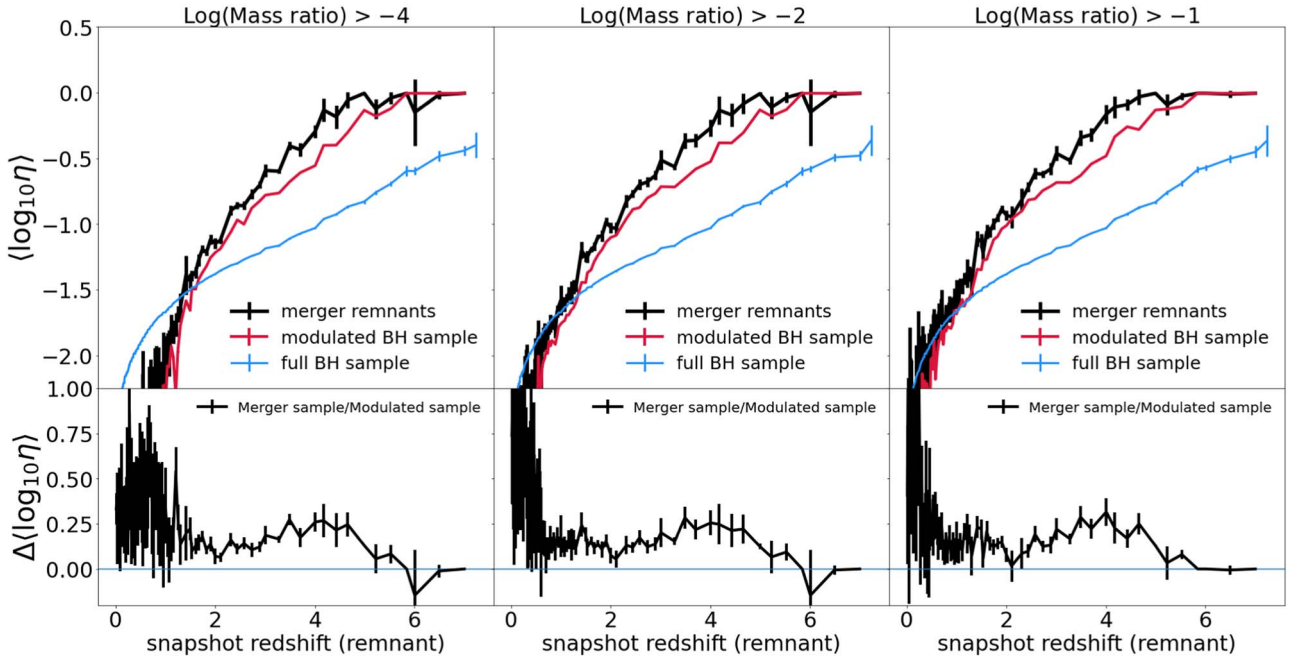

Figure 14. Upper panels: black lines show the median Eddington ratios of the complete sample of merger remnants at each simulation snapshot plotted as a function of the snapshot redshift. The blue lines correspond to the median Eddington ratio of the full sample of BHs at each snapshot. The red lines correspond to a subsample of BHs, which are modulated to have similar BH mass distributions as that of the merger remnants. We perform the modulation by subsampling the full population of BHs at different mass bins based on the fraction of merger remnants residing in the respective mass bins. We refer to this sample as the "modulated BH sample." The left to right panels correspond to increasing mass ratio between the secondary (less massive) vs. primary (more massive) progenitor BHs. For $z > 2$, we find that the merger remnants have higher Eddington ratios than the full population of BHs. For $z < 2$, the low mass ratio ($\sim 10^{-4}$–10^{-3}) systems have lower Eddington ratios than the full population of BHs; these systems correspond to primary BH masses $>10^9\,M_\odot/h$, wherein the kinetic AGN feedback drives out gas and suppresses the Eddington ratio. Lower panels: the ratio between the median Eddington ratios of merger remnants vs. the modulated BH sample, i.e., black vs. red lines in the top panels. Merger remnants have higher Eddington ratios (by factors up to $\sim$2) compared to random samples of BHs with similar masses.

enhanced Eddington ratios throughout the entire redshift range of $0 < z < 6$ compared to BHs of similar mass, but only up to factors of $\sim$2.

Overall, this is consistent with our results on BH systems, i.e., mergers do enhance AGN activity, but they are not the dominant drivers of AGN and BH growth.

ORCID iDs

Aklant K. Bhowmick https://orcid.org/0000-0002-7080-2864
Laura Blecha https://orcid.org/0000-0002-2183-1087

References

Armitage, P. J., & Natarajan, P. 2002, ApJL, 567, L9
Baker, J., Bellovary, J., Bender, P. L., et al. 2019, arXiv:1907.06482
Barnes, J., & Hut, P. 1986, Natur, 324, 446
Barnes, J. E., & Hernquist, L. 1996, ApJ, 471, 115
Barret, D., Nandra, K., Barcons, X., et al. 2013, in SF2A-2013: Proc. of the Annual meeting of the French Society of Astronomy and Astrophysics, ed. L. Cambresy et al. (Paris: Société Francaise d'Astronomie et d'Astrophysique), 447
Begelman, M. C., Blandford, R. D., & Rees, M. J. 1980, Natur, 287, 307
Bellovary, J. M., Governato, F., Quinn, T. R., et al. 2010, ApJL, 721, L148
Bhowmick, A. K., Di Matteo, T., & Myers, A. D. 2020, MNRAS, 492, 5620
Bhowmick, A. K., DiMatteo, T., Eftekharzadeh, S., & Myers, A. D. 2019, MNRAS, 485, 2026
Blecha, L., Loeb, A., & Narayan, R. 2013, MNRAS, 429, 2594
Blecha, L., Snyder, G. F., Satyapal, S., & Ellison, S. L. 2018, MNRAS, 478, 3056
Bonetti, M., Haardt, F., Sesana, A., & Barausse, E. 2016, MNRAS, 461, 4419
Bonetti, M., Sesana, A., Haardt, F., Barausse, E., & Colpi, M. 2019, MNRAS, 486, 4044
Bournaud, F., Dekel, A., Teyssier, R., et al. 2011, ApJL, 741, L33
Capelo, P. R., Volonteri, M., Dotti, M., et al. 2015, MNRAS, 447, 2123
Cappelluti, N., Brusa, M., Hasinger, G., et al. 2009, A&A, 497, 635
Chandrasekhar, S. 1943, ApJ, 97, 255
Chen, Y.-M., Wang, J.-M., Yan, C.-S., Hu, C., & Zhang, S. 2009, ApJL, 695, L130
Cisternas, M., Jahnke, K., Inskip, K. J., et al. 2011, ApJ, 726, 57
Comerford, J. M., Schluns, K., Greene, J. E., & Cool, R. J. 2013, ApJ, 777, 64
Davis, M., Efstathiou, G., Frenk, C. S., & White, S. D. M. 1985, ApJ, 292, 371
Desvignes, G., Caballero, R. N., Lentati, L., et al. 2016, MNRAS, 458, 3341
Di Matteo, T., Springel, V., & Hernquist, L. 2005, Natur, 433, 604
Donnari, M., Pillepich, A., Nelson, D., et al. 2019, MNRAS, 485, 4817
Eftekharzadeh, S., Myers, A. D., Hennawi, J. F., et al. 2017, MNRAS, 468, 77
Ellison, S. L., Mendel, J. T., Patton, D. R., & Scudder, J. M. 2013, MNRAS, 435, 3627
Ellison, S. L., Patton, D. R., Mendel, J. T., & Scudder, J. M. 2011, MNRAS, 418, 2043
Ellison, S. L., Viswanathan, A., Patton, D. R., et al. 2019, MNRAS, 487, 2491
Gabor, J. M., Impey, C. D., Jahnke, K., et al. 2009, ApJ, 691, 705
Gao, F., Wang, L., Pearson, W. J., et al. 2020, A&A, 637, A94
Glikman, E., Simmons, B., Mailly, M., et al. 2015, ApJ, 806, 218
Goulding, A. D., Greene, J. E., Bezanson, R., et al. 2018, PASJ, 70, S37
Gualandris, A., Read, J. I., Dehnen, W., & Bortolas, E. 2017, MNRAS, 464, 2301
Harms, R. J., Ford, H. C., Tsvetanov, Z. I., et al. 1994, ApJL, 435, L35
Hennawi, J. F., Strauss, M. A., Oguri, M., et al. 2006, AJ, 131, 1
Holley-Bockelmann, K., & Khan, F. M. 2015, ApJ, 810, 139
Hopkins, P. F., Hernquist, L., Cox, T. J., et al. 2006, ApJS, 163, 1
Hopkins, P. F., Hernquist, L., Cox, T. J., & Kereš, D. 2008, ApJS, 175, 356
Hou, M., Li, Z., & Liu, X. 2020, ApJ, 900, 79
Hou, M., Liu, X., Guo, H., et al. 2019, ApJ, 882, 41
Kayo, I., & Oguri, M. 2012, MNRAS, 424, 1363
Kelley, L. Z., Blecha, L., & Hernquist, L. 2017, MNRAS, 464, 3131
Khan, F. M., Holley-Bockelmann, K., Berczik, P., & Just, A. 2013, ApJ, 773, 100
Kocevski, D. D., Brightman, M., Nandra, K., et al. 2015, ApJ, 814, 104
Kocevski, D. D., Faber, S. M., Mozena, M., et al. 2012, ApJ, 744, 148
Kormendy, J., & Kennicutt, R. C. J. 2004, ARA&A, 42, 603
Kormendy, J., & Richstone, D. 1992, ApJ, 393, 559
Koss, M., Mushotzky, R., Treister, E., et al. 2011, ApJL, 735, L42
Koss, M., Mushotzky, R., Treister, E., et al. 2012, ApJL, 746, L22
Koss, M. J., Blecha, L., Bernhard, P., et al. 2018, Natur, 563, 214
Kovačević, A. B., Yi, T., Dai, X., et al. 2020, MNRAS, 494, 4069
Krumpe, M., Miyaji, T., Coil, A. L., & Aceves, H. 2018, MNRAS, 474, 1773
Kumar, P., & Johnson, J. L. 2010, MNRAS, 404, 2170
Lackner, C. N., Silverman, J. D., Salvato, M., et al. 2014, AJ, 148, 137
LaMassa, S. M., Urry, C. M., Glikman, E., et al. 2013, MNRAS, 432, 1351
Li, C., Kauffmann, G., Wang, L., et al. 2006, MNRAS, 373, 457
Liu, T., Gezari, S., Ayers, M., et al. 2019, ApJ, 884, 36
Liu, X., Shen, Y., Strauss, M. A., & Hao, L. 2011, ApJ, 737, 101
Lusso, E., Comastri, A., Simmons, B. D., et al. 2012, MNRAS, 425, 623
Manchester, R. N., Hobbs, G., Bailes, M., et al. 2013, PASA, 30, e017
Mannerkoski, M., Johansson, P. H., Pihajoki, P., Rantala, A., & Naab, T. 2019, ApJ, 887, 35
Marian, V., Jahnke, K., Mechtley, M., et al. 2019, ApJ, 882, 141
Marinacci, F., Vogelsberger, M., Pakmor, R., et al. 2018, MNRAS, 480, 5113
McAlpine, S., Harrison, C. M., Rosario, D. J., et al. 2020, MNRAS, 494, 5713
McGreer, I. D., Eftekharzadeh, S., Myers, A. D., & Fan, X. 2016, AJ, 151, 61
Milosavljević, M., & Merritt, D. 2003, in AIP Conf. Ser., 686, The Astrophysics of Gravitational Wave Sources, ed. J. M. Centrella (Melville, NY: AIP), 201
Miyoshi, M., Moran, J., Herrnstein, J., et al. 1995, Natur, 373, 127
Mushotzky, R. 2018, Proc. SPIE, 10699, 1069929
Nandra, K., Barret, D., Barcons, X., et al. 2013, arXiv:1306.2307
Nasim, I., Gualandris, A., Read, J., et al. 2020, MNRAS, 497, 739
Nelson, D., Pillepich, A., Genel, S., et al. 2015, A&C, 13, 12
Nelson, D., Pillepich, A., Springel, V., et al. 2018, MNRAS, 475, 624
Nelson, D., Pillepich, A., Springel, V., et al. 2019, MNRAS, 490, 3234
Ogiya, G., Hahn, O., Mingarelli, C. M. F., & Volonteri, M. 2020, MNRAS, 493, 3676
Oh, K., Koss, M., Markwardt, C. B., et al. 2018, ApJS, 235, 4
Pakmor, R., Bauer, A., & Springel, V. 2011, MNRAS, 418, 1392
Pakmor, R., Pfrommer, C., Simpson, C. M., Kannan, R., & Springel, V. 2016, MNRAS, 462, 2603
Perets, H. B., & Alexander, T. 2008, ApJ, 677, 146
Pfeifle, R. W., Satyapal, S., Manzano-King, C., et al. 2019, ApJ, 883, 167
Pillepich, A., Nelson, D., Hernquist, L., et al. 2018b, MNRAS, 475, 648
Pillepich, A., Nelson, D., Springel, V., et al. 2019, MNRAS, 490, 3196
Pillepich, A., Springel, V., Nelson, D., et al. 2017, MNRAS, 473, 4077
Pillepich, A., Springel, V., Nelson, D., et al. 2018a, MNRAS, 473, 4077
Planck Collaboration, Ade, P. A. R., Aghanim, N., et al. 2016, A&A, 594, A13
Powell, M. C., Urry, C. M., Cappelluti, N., et al. 2020, ApJ, 891, 41
Qu, Y., Helly, J. C., Bower, R. G., et al. 2017, MNRAS, 464, 1659
Quinlan, G. D. 1996, NewA, 1, 35
Rafikov, R. R. 2016, ApJ, 827, 111
Ransom, S., Brazier, A., Chatterjee, S., et al. 2019, BAAS, 51, 195
Ravi, V., Wyithe, J. S. B., Shannon, R. M., Hobbs, G., & Manchester, R. N. 2014, MNRAS, 442, 56
Ricci, C., Bauer, F. E., Treister, E., et al. 2017, MNRAS, 468, 1273
Rodriguez, C., Taylor, G. B., Zavala, R. T., et al. 2006, ApJ, 646, 49
Rodriguez-Gomez, V., Pillepich, A., Sales, L. V., et al. 2016, MNRAS, 458, 2371
Ryu, T., Perna, R., Haiman, Z., Ostriker, J. P., & Stone, N. C. 2018, MNRAS, 473, 3410
Sánchez-Salcedo, F. J., & Chametla, R. O. 2014, ApJ, 794, 167
Sanders, D. B., & Mirabel, I. F. 1996, ARA&A, 34, 749
Sanders, D. B., Soifer, B. T., Elias, J. H., et al. 1988, ApJ, 325, 74
Satyapal, S., Ellison, S. L., McAlpine, W., et al. 2014, MNRAS, 441, 1297
Schawinski, K., Simmons, B. D., Urry, C. M., Treister, E., & Glikman, E. 2012, MNRAS, 425, L61
Schaye, J., Crain, R. A., Bower, R. G., et al. 2015, MNRAS, 446, 521
Schneider, D. P., Fan, X., Strauss, M. A., et al. 2000, AJ, 120, 2183
Secrest, N., Ellison, S., Satyapal, S., & Blecha, L. 2020, MNRAS, 499, 2380
Sesana, A. 2010, ApJ, 719, 851
Silverman, J. D., Kampczyk, P., Jahnke, K., et al. 2011, ApJ, 743, 2
Snyder, G. F., Hayward, C. C., Sajina, A., et al. 2013, ApJ, 768, 168
Springel, V. 2010, MNRAS, 401, 791
Springel, V., & Hernquist, L. 2003, MNRAS, 339, 289
Springel, V., Pakmor, R., Pillepich, A., et al. 2018, MNRAS, 475, 676
Springel, V., Yoshida, N., & White, S. D. M. 2001, NewA, 6, 79
The Lynx Team 2018, arXiv:1809.09642
Urrutia, T., Lacy, M., & Becker, R. H. 2008, ApJ, 674, 80
Vasiliev, E., Antonini, F., & Merritt, D. 2015, ApJ, 810, 49
Vasudevan, R. V., Fabian, A. C., Gandhi, P., Winter, L. M., & Mushotzky, R. F. 2010, MNRAS, 402, 1081

Veilleux, S., Rupke, D. S. N., Kim, D. C., et al. 2009, ApJS, 182, 628
Verbiest, J. P. W., Lentati, L., Hobbs, G., et al. 2016, MNRAS, 458, 1267
Villforth, C., Hamann, F., Rosario, D. J., et al. 2014, MNRAS, 439, 3342
Villforth, C., Hamilton, T., Pawlik, M. M., et al. 2017, MNRAS, 466, 812
Vogelsberger, M., Genel, S., Sijacki, D., et al. 2013, MNRAS, 436, 3031
Vogelsberger, M., Genel, S., Springel, V., et al. 2014, MNRAS, 444, 1518
Vogelsberger, M., Nelson, D., Pillepich, A., et al. 2020, MNRAS, 492, 5167
Wang, L., & Li, C. 2019, MNRAS, 483, 1452
Weinberger, R., Springel, V., Hernquist, L., et al. 2017, MNRAS, 465, 3291
Weinberger, R., Springel, V., Pakmor, R., et al. 2018, MNRAS, 479, 4056
Weston, M. E., McIntosh, D. H., Brodwin, M., et al. 2017, MNRAS, 464, 3882
White, S. D. M. 1994, astro, arXiv:astro-ph/9410043
Yang, C., Ge, J., & Lu, Y. 2019, SCPMA, 62, 129511
Zakamska, N. L., Sun, A.-L., Strauss, M. A., et al. 2019, MNRAS, 489, 497
Zel'dovich, Y. B. 1970, A&A, 500, 13
Zhao, D., Ho, L. C., Zhao, Y., Shangguan, J., & Kim, M. 2019, ApJ, 877, 52